apoptotic morphological change of nuclei (nuclear condensation and fragmentation, Figure 5c) and cell death (Figure 5d) in the Doxo-sensitive SK-N-SH cells but not in the resistant IMR32 cells.

Doxo-induced stress induces mitochondrial dysfunction and activates the intrinsic caspase pathway

Next, we evaluated mitochondria homeostasis and activation of caspase pathways in NB cells. First, we investigated the role of mitochondrial membrane potential in Doxo-induced apoptosis. Mitochondrial membrane potential was assessed 10 h after Doxo stimulation by staining with the mitochondrion-selective dye, MitoTracker. Doxo-sensitive cells exhibited substantial mitochondrial depolarization, as evidenced by the loss of MitoTracker staining (Figure 6a). In contrast, depolarization was not induced by Doxo in the resistant cells. Next, immunofluorescence experiments showed that cytochrome-*c* was clearly released from mitochondria in the sensitive cells but not in the resistant cells (Figure 6b, Doxo-treated cells, 'Cyto. C' panels). Nuclear condensation was especially observed in the cells from which large amounts of cytochrome-*c* were released (Doxo-treated cells, 'Nuc' panels). These results suggest that mitochondrial dysfunction plays a pivotal role in Doxo-induced apoptosis in NB cells.

The central component of apoptosis is a proteolytic system involving a family of proteases called caspases (Green, 2000). As shown in Figure 6c, pro-caspase-9 cleavage was observed in the Doxo-sensitive cells, but not in the resistant cells 12 h after exposure to Doxo. The substrates of the activated caspase-9, pro-caspase-3 and -7 were also cleaved in the Doxo-sensitive cells. These findings suggest that apoptotic signals induced by Doxo activate the intrinsic caspase pathway via a mitochondrial pathway in NB cells, resulting in cell death of the Doxo-sensitive NB cells. Meanwhile, the resistant cells showed no activation of these initiator (caspase-9) and effector (caspase-3 and/or -7) caspases.

Discussion

Human *Noxa* is located on chromosome 18q21 and its promoter region contains a p53-responsive element (Oda *et al*., 2003). The expression of p53 increases human *Noxa* mRNA, and ectopic expression of Noxa effectively induces apoptosis in a BH3-motif-dependent manner (Oda *et al*., 2003). In the present study, we observed that Doxo-sensitive NB cells exhibited the Noxa mRNA/protein induction and protein localization into mitochondria after the treatment with Doxo, leading to an increase in the ratio of pro-/anti-apoptotic Bcl-2 family proteins. Mitochondrial dysfunction and intrinsic caspase-mediated apoptosis were also induced in the sensitive cells. Notably, apoptosis was almost completely canceled by the knockdown of Noxa by siRNA, confirming the importance of Noxa in the Doxo-induced apoptosis of NB cells. Taken together, these findings indicate that the Noxa upregulation in mitochondria may play an important role in Doxo-induced apoptosis in NB cells. A previous study described that Noxa and Bok were induced by etoposide, and *Noxa* siRNA treatment reduced etoposide-induced cell death in SH-SY5Y NB cells (Yakovlev *et al*., 2004). Furthermore, Obexer *et al*. (2007) reported that Noxa and Bim are effectors of FKHRL-1-induced apoptosis in NB cells. Since we also observed the upregulation of Noxa in mitochondria by Doxo or etoposide treatment, Noxa seems to be one of the important effectors of the pro-apoptotic signaling pathway in NB cell apoptosis.

Whereas Yakovlev *et al*. (2004) did not use stress-resistant NB cells, the kinetics of Noxa induction in the stress-resistant NB cells was evaluated in our study. In the Doxo-resistant NB cells, exposure to Doxo failed to increase the expression of Noxa and the other downstream molecules in mitochondria, although p53 was abundant in the nucleus before Doxo exposure and some of the p53 serine residues that regulate p53 stability and activity (Shieh *et al*., 1997; Oda *et al*., 2000) were efficiently phosphorylated in the resistant cells, as well as in the sensitive cells. These results suggest that the lack of some p53 function in the resistant NB cells results in the failure of apoptosis, even under the pressure of DNA damage, such as Doxo treatment. It is of interest that the amounts of *Noxa* mRNA and protein in the mitochondria were much larger in the unstimulated resistant cells than in the sensitive cells but not stimulated by Doxo treatment. Alternatively, the inability to upregulate Noxa transcription in response to Doxo may be related to resistance to the anthracycline in some NB cells. Large amounts of *Noxa* mRNA in a part of unfavorable NB primary tumor samples (Figure 4C) supported the observation of inactivity of accumulated Noxa in the resistant cells. The accumulation of Noxa in unstimulated NB cells seems to be p53 independent, as it was suggested by our experiments. Although several findings suggest that Noxa is induced via a p53-independent pathway in neuronal cells (Kiryu-Seo *et al*., 2005; Wong *et al*., 2005), the exact molecular pathway responsible for the p53-independent Noxa induction in NB remains to be elucidated. One possibility is the presence of other p53 family proteins, for example, p63 and p73 proteins in NB cells. Actually, p73-alpha is expressed in several NB cell lines, including IMR32 and NB19 cells, and p63, but not deltaNp63, is highly expressed at the transcriptional level in IMR32 cells (data not shown). The study of the physiological role of p63 and p73 proteins on Noxa expression and Doxo-induced NB cell death seems to be meaningful for research of NB cell death.

A previous report indicated that although Noxa expression mediated by adenovirus could not induce apoptosis in either wild-type or *p53*-knockout MEFs, its expression effectively enhanced the apoptotic response to etoposide or UV (Shibue *et al*., 2003), suggesting that Noxa induces apoptosis in concert with not only p53-dependent cellular signals, but also p53-independent cellular signals. Additionally, we found a significant increase of *Noxa* mRNA amounts in the tumor samples

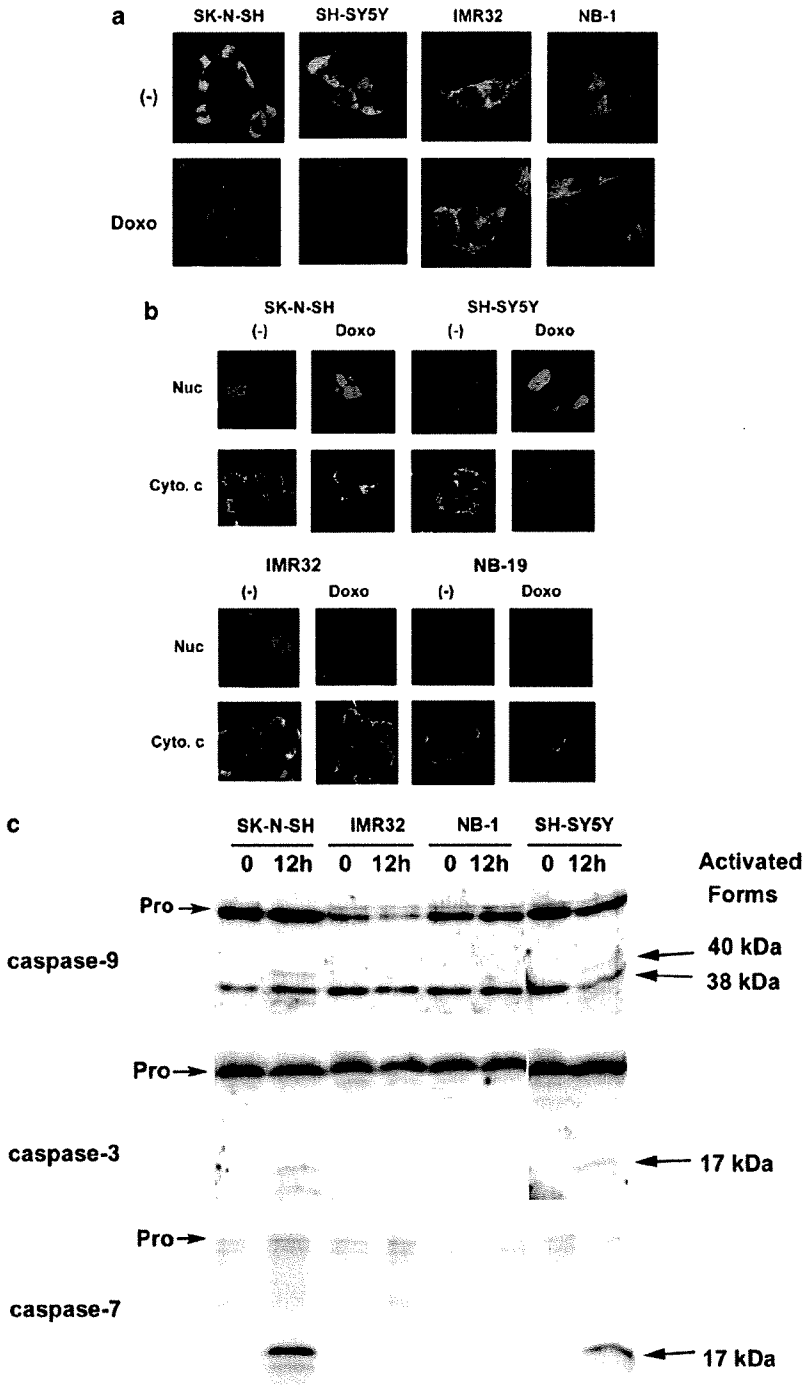

Figure 6 Mitochondrial dysfunction is induced by Doxo in the sensitive neuroblastoma (NB) cells. (**a**) Mitochondrial membrane potential was detected using MitoTracker dye 6 h after Doxo stimulation (Doxo). The steady-state potential is shown as a control [(−)]. (**b**) Cells were stimulated with Doxo for 6 h, and then cytochrome-*c* (Cyto. c) signals were detected by immunofluorescence experiments. The nucleus (Nuc) was stained with 4′,6-diamidino-2-phenylindole (DAPI). (**c**) Cells were collected at the indicated time points after Doxo stimulation and subjected to sodium dodecyl sulfate–polyacrylamide gel electrophoresis (SDS–PAGE)/western blot analysis. Processing of pro-caspase-9 was detected by the presence of 38/40-kDa cleaved forms. The anti-caspase-3 rabbit polyclonal antibody (BD Pharmingen) recognized the 32-kDa pro-caspase-3 and the 17-kDa cleaved form. The anti-caspase-7 mouse monoclonal antibody (clone B94-1) recognized the 35-kDa pro-caspase-7 and the 17-kDa cleaved form.

in the advanced stage (INSS3 and -4, younger than 12 months old) by quantitative real-time RT–PCR analysis (Figure 4D), indicating that the inactiveness of *Noxa* may relate to the progression in NB tumors. These observations suggest that reactivation of the accumulated Noxa in the Doxo-resistant NB cells with p53-independent stress may provide a new therapeutic approach to chemotherapy-resistant NB. Moreover, biochemical analysis of the accumulated Noxa in the mitochondria of resistant cells, for example, the analysis of Noxa-binding Bcl-2-family proteins in mitochondria, may be useful to address the mechanism of the failure of Doxo-induced apoptosis in those cells.

To address the other potential mechanisms of the resistances of DNA-damage-induced reagents in the chosen cell lines, we studied the genomic amplification of *MYCN* (Materials and methods), *caspase-8* and *P-glycoprotein* mRNA expression by semi-quantitative RT–PCR (data not shown). Caspase-8 was expressed in NB-9, NB-69, SK-N-SH and NB-1 cells. However, caspase-8 seems not to have a significant role in the Doxo-induced NB apoptosis, since we could not detect its activation by western blotting (data not shown). P-glycoprotein was clearly expressed in NB-9, NB-69, SK-N-SH and NB-1 cells, but not in SH-SY5Y, NB-1, and IMR32 cells (data not shown), suggesting that p-glycoprotein seems not to relate to the Doxo sensitivity of NB cells. Regarding *MYCN* amplification status, all the three resistant cell lines had *MYCN* amplification and three of four sensitive cell lines had single copy *MYCN*, suggesting that inactivity of p53 in the resistant cell lines may relate to the *MYCN* amplification. Consistent with our observation, Bell *et al.* (2006) reported that *MYCN* amplification correlates with attenuated $p21^{Cip1/Waf1}$ induction in *p53* wild-type NB cells. The analysis of the molecular mechanism between *MYCN* amplification and p53 inactivation in NB cells may be important for NB studies.

Taken together, our findings indicate that the p53 pathway regulates NB cell apoptosis via pro-apoptotic Noxa kinetics and localization in the mitochondria. Further study of Noxa in NB may provide an important approach to develop new therapies for NB and to improve the prognosis of high-risk NB patients.

Materials and methods

Reagents and antibodies

Anti-p53 mouse monoclonal antibody (clone DO-1), anti-Bcl-2 mouse monoclonal antibody (clone C-2), anti-$p21^{Cip1/Waf1}$ mouse monoclonal antibody (clone F-5) and anti-Bad mouse monoclonal antibody (clone C-7) were from Santa Cruz Biotechnology Inc. (Santa Cruz, CA, USA). Anti-cytochrome-*c* mouse monoclonal antibody (clone 7H8.2C12), anti-Bcl-xL mouse monoclonal antibody (clone 2H12), anti-caspase-3 rabbit polyclonal antibody, anti-caspase-7 mouse monoclonal antibody (clone B94-1) and anti-Bid rabbit polyclonal antibody were from BD PharMingen (San Diego, CA, USA). Anti-phospho-p53 rabbit serum (p53ser15p, p53ser20p and p53ser46p) and anti-phospho-p53ser15 mouse monoclonal antibody (clone 16G8) were from Cell Signaling Technology (Beverly, MA, USA). Anti-Bax and Anti-Bak rabbit polyclonal antibodies were from Upstate Biotechnology (Lake Placid, NY, USA). Anti-p53 mouse monoclonal antibody (clone pAb421), anti-p53 sheep polyclonal Antisera (Ab-7) Kit and anti-Noxa mouse monoclonal antibody (clone 114C307, for immunofluorescence analysis) were from Oncogene Research Products (Cambridge, MA, USA). Anti-Noxa rabbit polyclonal antibody (for western blotting) was from Abcam (Cambridge, UK). Anti-Bim rabbit polyclonal antibody was from Millennium Biotechnology (Ramona, CA, USA). Anti-Bok rabbit polyclonal antibody was from ABGENT (San Diego, CA, USA). Anti-caspase-9 mouse monoclonal antibody (clone 5B4) was from MBL (Nagoya, Japan). Anti-lamin monoclonal antibody (clone JOL2) was from Chemicon (Temecula, CA, USA). Anti-β-tubulin mouse monoclonal antibody (clone KMX-1) was from Roche Diagnostics (Manheim, Germany). Anti-trifunctional protein serum was prepared by rabbit immunization and affinity selection with purified trifunctional protein (Kamijo *et al.*, 1993). Anti-HDM2 monoclonal antibody (clone 2A10) was a generous gift from Dr Arnold J Levine, Pediatrics and Biochemistry Cancer Institute of New Jersey. Other biochemical reagents were purchased from Sigma-Aldrich Japan, or Wako (Osaka, Japan).

Cells and cell culture

We collected p53 wild-type NB cell lines to study the role of the p53 pathway in drug resistance mechanism of NB cells. SK-N-SH, NB-9, NB-19 and NB69 were obtained from Riken Cell Bank (Tsukuba, Japan). IMR32 and NB-1 were from Cell Resource Center for Biomedical Research Institute of Development, Aging and Cancer, Tohoku University. The wild-type *p53*-expressing SH-SY5Y line was purchased from ATCC (Manassas, VA, USA). The wild-type p53 status was demonstrated in previous reports (IMR32: Hopkins-Donaldson *et al.*, 2002; SK-N-SH: Wolff *et al.*, 2001) and p53 sequencing, which was performed according to the previous report (Tweddle *et al.*, 2001), confirmed the wild-type p53 status in these cell lines. In terms of the copy number of MYCN by Southern blot analysis, SH-SY5Y, SK-N-SH and NB-69 are single-copy NB cells; NB-9, IMR32, NB-1 and NB-19 cells have 50, >150, >150 and 25 copies, respectively (data not shown). The cells were routinely maintained with DMEM supplemented with 10% fetal bovine serum (FBS) and 1 × penicillin/streptomycin (Invitrogen, Carlsbad, CA, USA).

Tumor samples

Fresh, frozen tumor tissues were sent to the Division of Biochemistry, Chiba Cancer Center Research Institute, from various hospitals in Japan with informed consent from the patients' parents. All samples were obtained by surgery or biopsy and stored at −80°C. More than 70% of tumor cell contents of the samples were confirmed by pathological analysis of the adjacent tissues. Studies were approved by the Institutional Review Board of the Chiba Cancer Center.

Cell proliferation assay

NB cells were seeded in 96-well plates at a density of 10^4 cells/well in a final volume of 100 μl. Twenty-four hours after seeding, the medium was removed and replaced with fresh medium or with medium containing 0.5 μg/ml of Doxo or 20 μM etoposide in a final volume of 100 μl. The culture was maintained in the 5% CO_2 for 24 h and then 10 μl of WST-8 labeling solution (Cell Counting Kit-8, DOJINDO, Kumamoto, Japan) was added, and the cells were returned to the incubator for 4 h. The absorbance of the formazan product formed was

Table 1 Sequence of primers for PCR experiments

Gene	*Forward primer sequence*	*Reverse primer sequence*	*Accession number*
p53	cagccaagtctgtgacttgcacgtac	ctatgtcgaaaagtgtttctgtcatc	NM_000546
$p21^{Cip1/Waf1}$	gacaccactggagggtgact	ggcgtttggagtggtagaaa	L25610
HDM2	tagtagcattatttatagcagcc	agagaagaaatctatgtgaattgag	Z12020
Noxa	agagctggaagtcgagtgt	gcaccttcacattcctctc	D90070
Bax	ttttgcttcagggtttcatc	cagttgaagttgccgtcaga	BC014175
Bak1	gcctttgcagttggactctc	gggttgggagcaagtgtcta	NM_001188
IFN-α1	caatatctacgatggcctcgc	agagatggctggagccttctg	NM_024013
Caspase-8	gggacaggaatggaacacac	gccatagatgatgcccttgt	AF009620
P-glycoprotein	gaatctggaggaagacatgacc	tccaattttgtcaccaattcc	NM_000927
G3PDH	accacagtccatgccatcac	tccaccaccctgttgctgta	NM_002046

detected at 450 nm in a 96-well spectrophotometric plate reader, as per the manufacturer's protocol.

Morphological analysis of apoptosis and analysis of sub-G_0/G_1 fraction

Cells were observed using a phase-contrast microscope to assess apoptotic morphological changes and treated with 4′,6-diamidino-2-phenylindole (DAPI), a DNA-staining dye, to detect the morphological characteristics of apoptotic nuclei, namely, condensation and fragmentation, after fixation with 3.7% (v/v) formaldehyde/1 × phosphate-buffered saline (PBS). Analysis of sub-G_0/G_1 fraction was performed by using the method described in the previous report (Nakazawa *et al.*, 2003).

Immunofluorescence

Fixation was performed with 3.7% (v/v) formaldehyde/1 × PBS for 30 min and the permeabilization was done with 0.1% (v/v) TritonX-100/1 × PBS for 5 min at room temperature. Cells were then stained for 1 h with the first antibody followed by a 30-min exposure to an appropriate second antibody conjugated with fluorescent dye (Alexa488 or Alexa594). DNA was visualized with DAPI or propidium iodide. Analysis by confocal laser microscopy was performed with an LSM510 system (Carl Zeiss, Oberkochen, Germany).

Cell fractionation and direct western blotting

For the isolation of the heavy membrane faction (Mito) in Figures 4A and B, 2×10^6 cells were subjected to the fractionation procedure described previously (Nakazawa *et al.*, 2003). The resulting supernatant after isolation of Mito was referred to as the cytosol plus light membrane (Cyto) fractions.

For isolation of the nucleus (Nuc) in Figure 2d, 1×10^6 cells were suspended in 0.4 ml of buffer (10 mM HEPES pH 7.9, 10 mM KCl, 1.5 mM $MgCl_2$, 0.5 mM DTT, 0.4 μM PMSF), and incubated on ice for 20 min. After vortexing for 1 min at the maximum setting, cells were centrifuged at 15 000 r.p.m. for 10 s, and then the supernatant was kept as cytosol (Cyto). The pellet was resuspended in 0.1 ml of buffer (20 mM HEPES pH 7.9, 420 mM NaCl, 1.5 mM $MgCl_2$, 0.2 mM EDTA, 25% (v/v) glycerol, 0.5 mM DTT, 0.4 μM PMSF), and incubated on ice for 20 min. Then the cells were centrifuged at 15 000 r.p.m. for 2 min, and then the supernatant was kept as nucleus (Nuc). Direct western blotting was performed according to the previous report (Nakazawa *et al.*, 2003).

Preparation of mRNA and analysis of RNA expression

Total RNA was extracted from NB cells using Isogen (Wako, Tokyo, Japan), and cDNA was synthesized from 1 μg of total RNA templates according to the manufacturer's protocol (RiverTra-Ace-α- RT–PCR kit, TOYOBO, Osaka, Japan). PCR amplification of either p53 or Noxa was performed using previously reported primers (for p53: Paull and Whikehart, 2005; for Noxa: Ohtani *et al.*, 2004). The other primer sequences are listed in Table 1. RT–PCR products (~0.5 kb) were detected by direct ethidium bromide staining after electrophoretic separation on agarose gels. RT–PCR analysis of G3PDH mRNA expression was performed as a positive control for these experiments according to the manufacturer's protocol (RiverTra-Ace -α- RT–PCR kit). Semi-quantitative RT–PCR analysis of tumor samples was performed according to the previous report (Machida *et al.*, 2006). The PCR amplification was performed using the above-mentioned primers for Noxa.

Quantitative real-time PCR analysis

For quantification of Noxa in primary NB samples, cDNA was synthesized with random primers Superscript II reverse transcriptase (GibcoBRL) from 15 μg of primary tumor total RNA. Noxa and GAPDH primers and probes were purchased from Applied Biosystems (Noxa Assay ID: Hs00560402_m1; GAPDH: Pre-Developed TaqMan Assay Reagents Human G3PDH). Quantitative real-time PCR analysis was performed by ABI7700 Prism sequence detector (Applied Biosystems, Foster City, CA, USA), according to the manufacturer's instructions using 1 × TaqMan Universal PCR Master Mix. After denaturing at 95°C for 10 min, PCR amplification was performed by 50 cycles of denaturation at 95°C for 15 s and annealing/extension at 60°C for 1 min. A quantification of *Noxa* mRNA in each sample was performed by comparing with the standard curve, which was generated by reacting the plasmid containing human Noxa (Hijikata *et al.*, 1990). Furthermore, G3PDH mRNA quantification was also performed for a standardization of the initial RNA content of each sample.

Small interference RNA transfection

Noxa small interference RNAs were synthesized according to the previous experiments (Noxa siRNA1, Qin *et al.*, 2004: 5′-TCAGTCTACTGATTTACTGG-3′; Noxa siRNA2, Lee *et al.*, 2005: 5′-AACTTCCGGCAGAAACTTCTG-3′). Control siRNA (Silencer Negative Control #1 siRNA) was purchased from Ambion Inc. (Austin, TX, USA). NB cells were plated at a density of 3×10^5 cells in a 3-cm-diameter dish. Small interference RNA duplexes (10 nM) were transfected with Lipofectamine™ RNAiMAX in Opti-MEM medium according to the manufacturer's protocol. After 24 h, transfected cells were treated with Doxo for another 24 h.

Statistical analysis

The Welch test was used as a statistical method of parametric test to explore possible associations between Noxa expression and other factors, using StatView ver. 4.11 (Abacus Concepts

Inc., Cheltenham, UK). Statistical significance was declared if the P-value was <0.05.

Acknowledgements

We are deeply indebted to Professor Kenichi Koike (Department of Pediatrics, Shinshu University School of Medicine) for his excellent advice. We thank Kumiko Sakurai, Yozo Nakazawa, and Jun Miki for their technical assistance, and Daniel Mrozek, Medical English Service Inc, for editorial assistance. This work was supported by grants from the Japanese Ministry of Education, Science, Sports and Culture, Grant-in-Aid for Scientific Research (C) (contract nos: 15591098 and 17591077).

References

Aleyasin H, Cregan SP, Iyirhiaro G, O'Hare MJ, Callaghan SM, Slack RS *et al.* (2004). Nuclear factor-(kappa)B modulates the p53 response in neurons exposed to DNA damage. *J Neurosci* **24**: 2963–2973.

Bell E, Premkumar R, Carr J, Lu X, Lovat PE, Kees UR *et al.* (2006). The role of MYCN in the failure of MYCN amplified neuroblastoma cell lines to G1 arrest after DNA damage. *Cell Cycle* **5**: 2639–2647.

Danial NN, Korsmeyer SJ. (2004). Cell death: critical control points. *Cell* **116**: 205–219.

Green DR. (2000). Apoptotic pathways: paper wraps stone blunts scissors. *Cell* **102**: 1–4.

Hempel G, Flege S, Wurthwein G, Boos J. (2002). Peak plasma concentrations of doxorubicin in children with acute lymphoblastic leukemia or non-Hodgkin lymphoma. *Cancer Chemother Pharmacol* **49**: 133–141.

Hijikata M, Kato N, Sato T, Kagami Y, Shimotohno K. (1990). Molecular cloning and characterization of a cDNA for a novel phorbol-12-myristate-13-acetate-responsive gene that is highly expressed in an adult T-cell leukemia cell line. *J Virol* **64**: 4632–4639.

Hopkins-Donaldson S, Yan P, Bourloud KB, Muhlethaler A, Bodmer JL, Gross N. (2002). Doxorubicin-induced death in neuroblastoma does not involve death receptors in S-type cells and is caspase-independent in N-type cells. *Oncogene* **21**: 6132–6137.

Hudson CD, Morris PJ, Latchman DS, Budhram-Mahadeo VS. (2005). Brn-3a transcription factor blocks p53-mediated activation of proapoptotic target genes Noxa and Bax *in vitro* and *in vivo* to determine cell fate. *J Biol Chem* **280**: 11851–11948.

Isaacs JS, Saito S, Neckers LM. (2001). Requirement for HDM2 activity in the rapid degradation of p53 in neuroblastoma. *J Biol Chem* **276**: 18497–18506.

Kamijo T, Aoyama T, Miyazaki J, Hashimoto T. (1993). Molecular cloning of the cDNAs for the subunits of rat mitochondrial fatty acid beta-oxidation multienzyme complex. Structural and functional relationships to other mitochondrial and peroxisomal beta-oxidation enzymes. *J Biol Chem* **268**: 26452–26460.

Keshelava N, Zuo JJ, Chen P, Waidyaratne SN, Luna MC, Gomer CJ *et al.* (2001). Loss of p53 function confers high-level multidrug resistance in neuroblastoma cell lines. *Cancer Res* **61**: 6185–6193.

Kiryu-Seo S, Hirayama T, Kato R, Kiyama H. (2005). Noxa is a critical mediator of p53-dependent motor neuron death after nerve injury in adult mouse. *J Neurosci* **25**: 1442–1447.

Komarova EA, Chernov MV, Franks R, Wang K, Armin G, Zelnick CR *et al.* (1997). Transgenic mice with p53-responsive lacZ: p53 activity varies dramatically during normal development and determines radiation and drug sensitivity *in vivo*. *EMBO J* **16**: 1391–1400.

Letai A, Bassik MC, Walensky LD, Sorcinelli MD, Weiler S, Korsmeyer SJ. (2002). Distinct BH3 domains either sensitize or activate mitochondrial apoptosis, serving as prototype cancer therapeutics. *Cancer Cell* **2**: 183–192.

Lee SJ, Kim KM, Namkoong S, Kim CK, Kang YC, Lee H *et al.* (2005). Nitric oxide inhibition of homocysteine-induced human endothelial cell apoptosis by down-regulation of p53-dependent Noxa expression through the formation of S-nitrosohomocysteine. *J Biol Chem* **280**: 5781–5788.

Lowe SW, Bodis S, McClatchey A, Remington L, Ruley HE, Fisher DE *et al.* (1994). p53 status and the efficacy of cancer therapy *in vivo*. *Science* **266**: 807–810.

Machida T, Fujita T, Ooo ML, Ohira M, Isogai E, Mihara M *et al.* (2006). Increased expression of proapoptotic BMCC1, a novel gene with the BNIP2 and Cdc42GAP homology (BCH) domain, is associated with favorable prognosis in human neuroblastomas. *Oncogene* **25**: 1931–1942.

Matthay KK, Perez C, Seeger RC, Brodeur GM, Shimada H, Atkinson JB *et al.* (1998). Successful treatment of stage III neuroblastoma based on prospective biologic staging: a Children's Cancer Group study. *J Clin Oncol* **16**: 1256–1264.

Moll UM, LaQuaglia M, Bénard J, Riou G. (1995). Wild-type p53 protein undergoes cytoplasmic sequestration in undifferentiated neuroblastomas but not in differentiated tumors. *Proc Natl Acad Sci USA* **92**: 4407–4411.

Moll UM, Ostermeyer AG, Haladay R, Winkfield B, Frazier M, Zambetti G. (1996). Cytoplasmic sequestration of wild-type p53 protein impairs the G1 checkpoint after DNA damage. *Mol Cell Biol* **16**: 1126–1137.

Nakazawa Y, Kamijo T, Koike K, Noda T. (2003). ARF tumor suppressor induces mitochondria-dependent apoptosis by modulation of mitochondrial Bcl-2 family proteins. *J Biol Chem* **278**: 27888–27895.

Obexer P, Geiger K, Ambros PF, Meister B, Ausserlechner MJ. (2007). FKHRL1-mediated expression of Noxa and Bim induces apoptosis via the mitochondria in neuroblastoma cells. *Cell Death Diff* **14**: 534–547.

Oda E, Ohki R, Murasawa H, Nemoto J, Shibue T, Yamashita T *et al.* (2003). Noxa, a BH3-only member of the Bcl-2 family and candidate mediator of p53-induced apoptosis. *Science* **17**: 1053–1058.

Oda K, Arakawa H, Tanaka T, Matsuda K, Tanikawa C, Mori T *et al.* (2000). p53AIP1, a potential mediator of p53-dependent apoptosis, and its regulation by Ser-46-phosphorylated p53. *Cell* **102**: 849–862.

Ohtani S, Kagawa S, Tango Y, Umeoka T, Tokunaga N, Tsunemitsu Y *et al.* (2004). Quantitative analysis of p53-targeted gene expression and visualization of p53 transcriptional activity following intratumoral administration of adenoviral p53 *in vivo*. *Mol Cancer Ther* **3**: 93–100.

Oren M. (1999). Regulation of the p53 tumor suppressor protein. *J Biol Chem* **274**: 36031–36034.

Paull AC, Whikehart DR. (2005). Regulation of the p53 tumor suppressor protein. *Mol Vis* **11**: 328–334.

Qin JZ, Stennett L, Bacon P, Bodner B, Hendrix MJ, Seftor RE *et al.* (2004). p53-independent NOXA induction overcomes apoptotic resistance of malignant melanomas. *Mol Cancer Ther* **3**: 895–902.

Shen Y, White E. (2001). p53-dependent apoptosis pathways. *Adv Cancer Res* **82**: 55–84.

Shibue T, Takeda K, Oda E, Tanaka H, Murasawa H, Takaoka A *et al.* (2003). Integral role of Noxa in p53-mediated apoptotic response. *Genes Dev* **17**: 2233–2238.

Shieh SY, Ikeda M, Taya Y, Prives C. (1997). DNA damage-induced phosphorylation of p53 alleviates inhibition by MDM2. *Cell* **91**: 325–334.

Tweddle DA, Malcolm AJ, Bown N, Pearson AD, Lunec J. (2001). Evidence for the development of p53 mutations after cytotoxic therapy in a neuroblastoma cell line. *Cancer Res* **61**: 8–13.

Tweddle DA, Pearson AD, Haber M, Norris MD, Xue C, Flemming C *et al.* (2003). The p53 pathway and its inactivation in neuroblastoma. *Cancer Lett* **197**: 93–98.

Wong HK, Fricker M, Wyttenbach A, Villunger A, Michalak EM, Strasser A *et al.* (2005). Mutually exclusive subsets of BH3-only proteins are activated by the p53 and c-Jun N-terminal kinase/c-Jun signaling pathways during cortical neuron apoptosis induced by arsenite. *Mol Cell Biol* **25**: 8732–8747.

Wei MC, Zong WX, Cheng EH, Lindsten T, Panoutsakopoulou V, Ross AJ *et al.* (2001). Proapoptotic BAX and BAK: a requisite gateway to mitochondrial dysfunction and death. *Science* **292**: 727–730.

Wolff A, Technau A, Ihling C, Technau-Ihling K, Erber R, Bosch FX *et al.* (2001). Evidence that wild-type p53 in neuroblastoma cells is in a conformation refractory to integration into the transcriptional complex. *Oncogene* **20**: 1307–1317.

Yakovlev AG, Di Giovanni S, Wang G, Liu W, Stoica B, Faden AI. (2004). BOK and NOXA are essential mediators of p53-dependent apoptosis. *J Biol Chem* **279**: 28367–28374.

British Journal of Cancer (2008) 99, 1891 – 1899

www.bjcancer.com

Loss of imprinting of *IGF2* correlates with hypermethylation of the *H19* differentially methylated region in hepatoblastoma

S Honda[1,4], Y Arai[2], M Haruta[1], F Sasaki[3], M Ohira[3], H Yamaoka[3], H Horie[3], A Nakagawara[3], E Hiyama[3], S Todo[4] and Y Kaneko*[,1,3]

[1]*Department of Cancer Diagnosis, Saitama Cancer Center, Research Institute for Clinical Oncology, 818 Komuro, Ina, Saitama 362-0806, Japan;* [2]*Cancer Genomics Project, National Cancer Center Research Institute, Chuo-Ku, Tokyo 104-0045, Japan;* [3]*Japanese Study Group for Pediatric Liver Tumor (JPLT), Hiroshima 734-8551, Japan;* [4]*Department of General Surgery, Hokkaido University Graduate School of Medicine, Sapporo 060-8638, Japan*

IGF2, a maternally imprinted foetal growth factor gene, is implicated in many childhood tumours including hepatoblastoma (HB); however, the genetic and epigenetic alterations have not comprehensively been studied. We analysed the methylation status of the *H19* differentially methylated region (DMR), loss of heterozygosity (LOH) and allelic expression of *IGF2* in 54 *HB* tumours, and found that 12 tumours (22%) with LOH, 9 (17%) with loss of imprinting (LOI) and 33 (61%) with retention of imprinting (ROI). Biallelic and monoallelic *IGF2* expressions correlated with hypermethylation and normal methylation of *H19* DMR, respectively, in two tumours with LOI and seven tumours with ROI. Quantitative RT–PCR analysis showed minimal expression of *H19* mRNA and substantial expression of *IGF2* mRNA in tumours with LOH or LOI, and substantial expression of both *H19* and *IGF2* mRNAs in tumours with ROI. Increased *IGF2* expression with predominant embryonic P3 transcript was found in the majority of HBs with ROI and foetal livers. In contrast to the earlier reports, our findings suggest that the disruption of the enhancer competition model reported in Wilms' tumour may also occur in HB. Both frequencies of LOH and LOI seem to be lower in HB than in Wilms' tumour, reflecting the different tissue origins.

British Journal of Cancer (2008) **99,** 1891 – 1899. doi:10.1038/sj.bjc.6604754 www.bjcancer.com
Published online 28 October 2008

Keywords: hepatoblastoma; *IGF2*; *H19*; loss of heterozygosity; loss of imprinting

Hepatoblastoma (HB) is a rare malignant neoplasm of the liver, with an incidence of 0.5–1.5 per million children (Perilongo and Shafford, 1999). Remarkable progress in clinical outcome has been achieved in the past 20 years because of advances in chemotherapy and surgical procedures; however, the mortality rate remains 20–30% and treatment results in patients in advanced stages who are refractory to standard preoperative chemotherapy regimens are unsatisfactory (Perilongo *et al*, 2000; Fuchs *et al*, 2002). To improve the mortality of these patients, innovative treatment based on a specific molecular target is needed. The molecular mechanism involved in the development and progression of HB includes overexpression of insulin-like growth factor-II (*IGF2*) (Li *et al*, 1998b; Gray *et al*, 2000; Hartmann *et al*, 2000), downregulation of *RASSF1A* by promoter hypermethylation (Sugawara *et al*, 2007; Honda *et al*, 2008) and alterations of genes in the Wnt signalling pathway; most notably, the high incidence of *CTNNB1* (catenin, β1) mutation (Koch *et al*, 1999; Taniguchi *et al*, 2002).

IGF2 is a maternally imprinted gene and encodes a foetal peptide hormone that regulates cellular proliferation and differentiation (Foulstone *et al*, 2005). *IGF2* has four promoter regions and P3 is the most active promoter in the foetal liver, followed by P2 and P4 promoters (Li *et al*, 1998a). *PLAG1* encodes a developmentally regulated transcription factor, which positively regulates *IGF2* through binding the P3 promoter region. Although *IGF2* is downregulated in normal tissues after birth, except for liver tissues, it is overexpressed in a wide variety of childhood and adult cancers and serves as a tumour enhancer through autocrine and paracrine mechanisms (Toretsky and Helman, 1996). *IGF2* has been studied extensively over the past decade as a key molecule involving HB and Wilms' tumour (WT) pathogenesis.

The allelic expression of *IGF2* is regulated by the methylation status of the sixth CTCF (CCCTC-binding factor) site in the *H19* differentially methylated region (DMR) that represents the parental origin of the *IGF2* allele; whereas the paternal CTCF6 allele is methylated, the maternal allele is unmethylated in normal tissues (Bell and Felsenfeld, 2000; Hark *et al*, 2000; Takai *et al*, 2001). Using the enhancer competition model, *IGF2* and *H19* promoters compete on the same chromosome for a shared enhancer, and access of the maternal *IGF2* allele to this enhancer is blocked by *H19* DMR when unmethylated because of the insulator activity of CTCF binding to unmethylated *H19* DMR (Bell and Felsenfeld, 2000; Hark *et al*, 2000). It has been proved in many WTs that aberrant methylation of the maternal CTCF6 prevents the insulator binding and leads to loss of imprinting (LOI), resulting in the overexpression of *IGF2* (Steenman *et al*, 1994; Ravenel *et al*, 2001). Although LOI of *IGF2* was reported in HB, the mechanism of LOI, the concurrent overexpression of *IGF2* mRNA and loss of

*Correspondence: Dr Y Kaneko; E-mail: kaneko@cancer-c.pref.saitama.jp
Received 24 June 2008; revised 30 September 2008; accepted 1 October 2008; published online 28 October 2008

H19 mRNA expression are uncertain because of the limited number of HB tumours examined and the low frequency of the heterozygous *IGF2* polymorphic site in general populations (Davies, 1993; Montagna *et al*, 1994; Rainier *et al*, 1995; Li *et al*, 1995, 1998b; Fukuzawa *et al*, 1999; Gray *et al*, 2000; Hartmann *et al*, 2000; Ross *et al*, 2000; Albrecht *et al*, 2004; Suzuki *et al*, 2008), and some investigators stated earlier that the mechanisms of *IGF2* upregulation by LOI found in WT do not apply to HB (Li *et al*, 1995; Hartmann *et al*, 2000).

Loss of imprinting was reported in 32–38% of WTs (Ravenel *et al*, 2001; Fukuzawa *et al*, 2004; Yuan *et al*, 2005), and loss of heterozygosity (LOH), leading to uniparental disomy (UPD) of the paternal *IGF2*, was reported in 36–50% of WTs (Grundy *et al*, 1996; Fukuzawa *et al*, 2004; Yuan *et al*, 2005). In HB, although LOH of *IGF2* was reported in 20–30%, the incidence of LOI of *IGF2* was uncertain because each series included only a small number of HB tumours. In addition, it is also uncertain whether the same mechanism of LOI is involved in both WT and HB tumorigeneses because the methylation status of *H19* DMR in HB has rarely been examined (Li *et al*, 1995, 1998b; Fukuzawa *et al*, 1999).

To determine whether the alterations of *IGF2* and *H19* loci identified in WT are also found in HB, we examined the LOI and LOH status of *IGF2* using combined bisulphite restriction assay (COBRA) of the CTCF6 region that can determine the methylation status of *H19* DMR more efficiently than the method using methylation-specific restriction enzymes and Southern blot in 54 HB tumours. In addition, we evaluated promoter-specific *IGF2* transcripts, the methylation status of *IGF2* promoters and *PLAG1* mRNA expression. Our results showed that the genetic and epigenetic alterations in the *IGF2-H19* region with elevated expression of *IGF2* mRNA identified in WTs were also found in the great majority of HB tumours, although the incidences of LOH and LOI may be lower in HBs than in WTs.

MATERIALS AND METHODS

Patients and samples

Tumour tissues were obtained from 54 Japanese children with HB, and adjacent normal liver tissues were available from 5 patients. Eighteen tumour and five matched normal liver specimens were supplied by the Tissue Bank of the Japanese Study Group for Pediatric Liver Tumour (JPLT) (Matsunaga *et al*, 2004), and 36 were supplied by institutions affiliated with Saitama Cancer Center. DNA and RNA were extracted from tumour and normal tissue samples that were immediately frozen after the resection or on arrival at the centre. The median age of the 54 patients at diagnosis was 18 months (range, 1–156 months). None of patients had the Beckwith–Wiedemann syndrome or a family history of familial polyposis coli. A total of 14 and 37 tumours were obtained before and after chemotherapy, respectively, and the chemotherapy status was unknown in the other 3 tumours. Pathologists in each institution and/or the JPLT pathology panel made the diagnosis of HB and verified that each sample contained 70% or more tumour cells. Informed consent was obtained from the parents, and the study design was approved by the ethics committee of Saitama Cancer Center.

COBRA of the CTCF6 site at *H19* DMR

We performed COBRA to determine the methylation status of the CTCF6 binding site at *H19* DMR, as described earlier (Watanabe *et al*, 2007). COBRA of CTCF6 showed that the mean methylation percentage ±2 s.d. of five normal livers was 52.8 ± 15.0%, and we defined more than the mean percentage +2 s.d. as the hypermethylated state.

LOH analysis of *IGF2*

High-resolution single nucleotide polymorphism (SNP) array, Affymetrix Mapping 50K-Xba array (Affymetrix, Santa Clara, CA, USA), was used to analyse chromosomal aberrations of 11p15.5 where *IGF2* resides. Genomic DNA in 43 of 54 tumours and 2 cell lines was assayed according to the manufacturer's protocol, and the genomic status of *IGF2* was determined as described earlier (Haruta *et al*, 2008).

Allelic expression analysis of *IGF2* and quantitative real-time reverse transcription-PCR analysis of *IGF2* and *H19* mRNA

The *ApaI*/*Ava*II polymorphic site in exon 9 of *IGF2* was used to evaluate the allelic expression of *IGF2* mRNA in 21 tumours whose RNA was available for this study, as described earlier (Watanabe *et al*, 2006). Quantitative real-time reverse transcription-PCR was performed to evaluate the total *IGF2* and *H19* mRNA levels in 20 tumour tissues, 2 HB cell lines (HuH6 and HepG2), foetal liver total RNA pooled from 34 foetuses (Clontech, Ohtsu, Japan) and 3 normal liver tissues adjacent to HB; the age of the patients was 16, 24 or 26 months. Of the 20 tumours, 3 and 16 were obtained before and after chemotherapy, respectively, and the chemotherapy status was unknown in 1. The primers and TaqMan probes used for *IGF2* and *H19* mRNA were described earlier (Watanabe *et al*, 2007; Haruta *et al*, 2008). The expression of *IGF2* and *H19* mRNAs was normalised with *GAPDH*.

Methylation-specific PCR and bisulphite sequencing analysis of *IGF2* promoter regions

Genomic DNA from tumour and normal liver samples was treated with sodium bisulphite (Herman *et al*, 1996), and the methylation status of the P2–P4 promoter regions of *IGF2* was analysed by methylation-specific PCR (MSP), as described earlier (Beeghly *et al*, 2007). Polymerase chain reaction products were run on 2% agarose gels and visualised after staining with ethidium bromide. We confirmed the results of MSP analysis of P3 promoter by bisulphite sequencing of eight or more subcloned plasmids.

Semiquantitative RT–PCR analysis of promoter-specific transcripts of *IGF2* and *PLAG1*

P1 and P3 promoter specific expressions of *IGF2* mRNA were analysed using the primer sets described elsewhere (Lu *et al*, 2006). The primer sequences for P2-specific transcript were derived from exons 4 and 5: forward, 5′-CCCTCAGGACGTGGACAG-3′; reverse, 5′-GTGCGTTGGACTTGCATAGA-3′; and the primer sequences for P4-specific transcript were derived from exons 7, 8 and 9: forward, 5′-CGAGCCTTCTGCTGAGCTAC-3′; reverse, 5′-CGGAAACAGCA CTCCTCAAC-3′. *PLAG1* mRNA expression was analysed using the following primer sets: forward, 5′-AACGTAAGCGTGGTGAAACC-3′; reverse, 5′-TGCCACATTCTTCGCACTTA-3′ (Zatkova *et al*, 2004). Polymerase chain reaction products were run on polyacrylamide gels and visualised after ethidium bromide staining. The intensity of each band was examined using a fluorescence image analyser, FLA-3000G (Fujifilm, Tokyo, Japan). Dividing the intensity of the target transcript by that of *GAPDH* calculated the level of each transcript.

Mutation analysis of the *CTNNB1* gene

To detect point mutations and deletions of the *CTNNB1* gene, genomic DNA from each tumour sample was amplified using two sets of primers, F1, 5′-TGGCTATCATTCTGCTTTTCTTG-3′ and R1, 5′-CTCTTTTCTTCACCACAACATTTT-3′, and BCAT-3, 5′-AA

AATCCAGCGTGGACAATGG-3′ and BCAT-4, 5′-TGTGGCAAGTT CTGCATCATC-3′, respectively (Koch *et al*, 1999; Satoh *et al*, 2003). The PCR products were either directly sequenced or inserted into a vector (pGEM (R)-T Easy Vector System (Promega, Madison, WI, USA)), and six or more clones were sequenced.

Statistical analysis

Student's *t*-test or Welch's *t*-test compared mRNA levels of *IGF2* and *H19* between tumours with or without *IGF2* alterations or other characteristics and the levels of *IGF2* promoter-specific transcripts between tumours with or without *PLAG1* mRNA expression. We also assessed the association between total *IGF2* mRNA levels and P2-, P3- or P4-specific *IGF2* mRNA levels by determining the Spearman rank correlation coefficient and associated *P*-value. Differences in the incidence of tumours with unmethylated P3 promoter were examined between tumours with hypermethylated *H19* DMR and tumours with normally methylated *H19* DMR by the χ^2 test. Differences in the incidences of tumours with *CTNNB1* mutation were examined between any two of three groups of tumours classified on the basis of the *IGF2* status by the χ^2 test.

RESULTS

Methylation status of the CTCF6 binding site at *H19* DMR, LOH analysis using SNP array and allelic expression analysis of *IGF2*

Combined bisulphite restriction assay showed that 21 and 33 tumours had hypermethylation and normal methylation at CTCF6, indicating LOH or LOI and retention of *IGF2* imprinting (ROI), respectively (Table 1 and Figure 1). Single nucleotide polymorphism array analysis was performed in 43 of 54 tumours; all 21 tumours with hypermethylated CTCF6 and 22 of 33 tumours with normally methylated CTCF6. Combined results of both analyses indicated that 12 tumours had LOH (10 hypermethylated CTCF6 and UPD 2 hypermethylated CTCF6 and hemizygous 11p15 deletion), 9 had LOI (hypermethylated CTCF6 and retention of heterozygosity (ROH)) and 22 had ROI (normally methylated CTCF6 and ROH). Of 21 tumours whose RNA was available, 9 and 12 tumours had heterozygous and homozygous *ApaI*/*Ava*II sites in exon 9 of *IGF2*, respectively. Of the nine heterozygous tumours, seven showed monoallelic expression of *IGF2*, indicating ROI, and two showed biallelic expression of *IGF2*, indicating LOI, and the results were consistent with those examined by COBRA and SNP array analyses (Table 1). From these findings, 11 tumours with normally methylated CTCF6, in which SNP array analysis was not performed, were classified as those with ROI. Thus, combined results of COBRA, SNP array and allelic expression analyses showed 12 tumours with LOH, 9 tumours with LOI and 33 tumours with ROI. In addition, one cell line (HuH6) had LOI, and the other (HepG2) had LOH (UPD) of *IGF2*.

The mean age was compared between any two of three groups of patients (i.e., LOH, LOI or ROI) by Student's *t*-test. There was no difference in the mean age between any two of the three groups of patients.

Correlation between *IGF2* and *H19* mRNA levels and the *IGF2* status (LOH, LOI or ROI)

Quantitative real-time reverse transcription-PCR analysis showed that although 15 of 20 tumours had a higher level of *IGF2* mRNA than normal liver tissues, 15 of 20 tumours had a lower level of *H19* mRNA than normal liver tissues (Table 1 and Figure 2). All 3 tumours with UPD, 1 of 1 with 11p15 loss, 1 of 3 with LOI and 10 of 13 with ROI, expressed higher levels of *IGF2* mRNA than normal liver tissues. There was no significant difference in *IGF2* mRNA levels between 3 tumours with UPD or 7 tumours with *IGF2* alterations; that is UPD, 11p15 loss or LOI, and 13 tumours with ROI. In contrast, 7 tumours with *IGF2* alterations expressed very low levels of *H19* mRNA, whereas 11 of 13 tumours with ROI expressed a substantial amount of *H19* mRNA; 2 tumours (nos. 25 and 27) with ROI expressed very low levels of *H19* mRNA. *H19* mRNA levels were higher in 13 HB tumours with ROI than in 7 HB tumours with *IGF2* alterations ($P<0.01$ by Welch's *t*-test). Although HepG2 with UPD had a higher level of *IGF2* mRNA than normal liver tissues, HuH6 with LOI had a very low level of *IGF2* mRNA. *H19* mRNA levels were very low in both cell lines.

Semiquantitative RT-PCR analysis of promoter-specific *IGF2* transcripts

Because the *IGF2* gene has four kinds of promoters, promoter-specific *IGF2* transcripts were analysed to determine the usage of each promoter. Representative results of the P3 transcript are shown in Figure 3A. All 20 tumours showed undetectable or lower levels of P1 transcripts than 3 normal liver tissues. The levels of P2, P3 and P4 transcripts were higher in 13, 15 and 10 of the 20 tumours, respectively, than those of normal liver tissues. Polymerase chain reaction cycle numbers to obtain visible levels of PCR products were 40 for P2 transcripts, 30 for P3 transcripts and 35 for P4 transcripts, indicating that the amounts of P3 transcripts were high, those of P2 transcripts were low and those of P4 transcripts were intermediate. The Spearman correlation coefficient analysis showed that the expression levels of the P2, P3 and P4 transcripts correlated with the levels of total *IGF2* mRNA (P2, $rS=0.730$; P3, $rS=0.773$ and P4, $rS=0.646$) (Figure 3B and C; data for the P2 and P4 transcripts are not shown).

The methylation status of *IGF2* promoters and its correlation with the levels of promoter-specific transcripts

In the MSP analysis of each promoter, the P2 promoter region was partially methylated in 19 tumours and normal liver tissues and the P4 promoter region was unmethylated in all 20 tumours and normal liver tissues. Therefore, the methylation status of P2 or P4 promoter region was not correlated with the expression level of P2- or P4-specific transcripts. The P3 promoter region was partially methylated in 11 tumours, HuH6 and normal liver tissues and unmethylated in 9 tumours and HepG2 (Table 1, Figure 4A and B). The results of MSP analysis in one tumour (no. 1) and HuH6 were confirmed by bisulphite sequencing (Figure 4C). Nine tumours with the unmethylated P3 promoter had higher levels of P3 transcripts than 11 tumours with the partially methylated P3 promoter ($P=0.005$) (Figure 4D). The P3 promoter was unmethylated in 5 of 7 tumours with *IGF2* alterations; UPD, 11p15 loss or LOI, but in 4 of 13 tumours with ROI. Thus, the incidence of tumours with unmethylated P3 promoter tended to be higher in tumours with hypermethylated *H19* DMR than in tumours with normally methylated *H19* DMR ($P=0.1$).

Semiquantitative RT-PCR analysis of *PLAG1* mRNA

PLAG1 positively regulates *IGF2*, and its expression was detected in 12 tumours, foetal liver RNA and 2 cell lines, but not in 8 tumour and 3 normal liver tissues (Table 1 and Figure 5). The 12 tumours with *PLAG1* mRNA expression showed higher levels of P4-specific *IGF2* transcripts ($P=0.01$) and tended to show higher levels of P3-specific *IGF2* transcripts ($P=0.051$) than the 8 tumours without *PLAG1* expression. There was no significant difference in P2- or P1-specific transcript levels between tumours with and without *PLAG1* mRNA expression.

Table 1 Genetic and epigenetic status of the *IGF2-H19* region in 54 hepatoblastoma tumours

Patients number	Age[a]/sex	Chemo[b]	%methyl CTCF6[c]	11p15 SNP[d]	*ApaI* site[e]	*IGF2* RT-PCR	*IGF2* status[f]	*IGF2* mRNA	P1E[g]	P2M[h]	P2E	P3M	P3E	P4E	*H19* mRNA	*PLAG1* mRNA	*CTNNB1* status[i]
1	48/F	+	82.8	UPD	Homo	ND	UPD	11.3	0.6	MU	17.7	U	7	3.1	0	+	M
2	5/M	–	93.4	UPD	Homo	ND	UPD	3.9	0	MU	0	U	2.1	0.9	0	–	M
3	24/M	+	76.7	UPD	Homo	ND	UPD	3.2	0	MU	2.4	MU	2.3	1.2	0	+	M
4–10	5–96/M6, F1	+6, –1	72–90	UPD	ND	ND	UPD	ND	ND	ND	ND	ND	ND	ND	ND	ND	M4, N3
11	27/M	+	87.8	Loss chr 11	Homo	ND	Loss	6.1	0	MU	2.3	U	4.4	1.3	0	+	M
12	24/M	+	81.9	Loss chr 11	ND	ND	Loss	ND	ND	ND	ND	ND	ND	ND	ND	ND	M
13	12/F	+	91.4	ROH	Homo	ND	LOI (m)	9.7	0	U	1.1	U	2.3	0.6	0	–	ND
14	16/M	–	86.1	ROH	Homo	ND	LOI (m)	1	0	MU	0.3	U	1.3	0.9	0	–	ND
15	26/F	+	83.1	ROH	Hetero	LOI	LOI (m, p)	0.8	0	MU	0.4	MU	0.6	0.9	0	–	M
16	24/M	+	70.9	ROH	Hetero	LOI	LOI (m, p)	ND	ND	ND	ND	ND	ND	ND	ND	ND	M
17–21	12–84/M4, F1	+1, –3, UK1	71–91	ROH	ND	ND	LOI (m)	ND	ND	ND	ND	ND	ND	ND	ND	ND	M3,N2
22	12/F	+	52.5	ND	Homo	ND	ROI (m)	9.2	0.8	MU	8.4	MU	2.8	2.2	3.5	+	N
23	109/F	+	49.1	ND	Homo	ND	ROI (m)	8.4	0	MU	4.3	U	4.6	2.8	0.5	+	M
24	12/M	–	56.3	ND	Hetero	ROI	ROI (m, p)	7.4	0	MU	13.2	U	4.6	2.4	1.9	+	M
25	15/M	+	55.9	ROH	Hetero	ROI	ROI (m, p)	5.7	0	MU	6.5	MU	5.1	2.2	0	+	ND
26	6/M	UK	51.1	ND	Hetero	ROI	ROI (m, p)	5.6	0.1	MU	4.7	U	1.2	0.5	2.7	+	ND
27	10/M	+	62.1	ROH	Homo	ND	ROI (m)	5	0	MU	0.9	U	5	1.1	0	–	ND
28	29/F	+	61.5	ND	Homo	ND	ROI (m)	3.7	0	MU	1.5	MU	2.5	1.4	2.5	+	M
29	26/M	+	55.4	ND	Homo	ND	ROI (m)	3.1	0.2	MU	9.3	MU	0.4	1.2	0.7	–	M
30	18/M	+	48.7	ND	Hetero	ROI	ROI (m, p)	2.4	0.1	MU	1.2	MU	1.1	1	0.8	–	ND
31	13/M	+	55.3	ND	Hetero	ROI	ROI (m, p)	2.2	0	MU	1.1	MU	1.5	1	0.6	+	N
32	60/F	+	55.7	ND	Hetero	ROI	ROI (m, p)	0.7	0.2	MU	0.2	MU	0.3	0.9	0.4	+	N
33	29/M	+	56.4	ND	Homo	ND	ROI (m)	0.5	1	MU	0.1	MU	0	0.5	1.2	–	M
34	9/M	+	56.7	ND	Hetero	ROI	ROI (m, p)	0.5	0	MU	0	MU	0.1	0.2	0.2	+	M
35–54	4–156/M11, F9	+12, –7, UK1	41–65	ROH	ND	ND	ROI (m)	ND	ND	ND	ND	ND	ND	ND	ND	ND	M11, N9
Normal livers			52.8	ND	ND	ND	ROI (m)	1	1	MU	1	MU	1	1	1	–	
Fetal livers			ND		ND	ND	ND	5.9	0.2	ND	6.4	ND	4.8	1.9	2.4	ND	
HuH6			87.3	ROH	Hetero	LOI	LOI (m, p)	0	0	MU	0	MU	0	0.1	0	+	M
HepG2			89.5	UPD	Homo	ND	UPD (m)	2.4	0	U	1.5	U	5	2.8	0	+	M

F = female; M = male; M = methylated; ROH = retention of heterozygosity; ROI = retention of imprinting; U = unmethylated; ND = not done; UK = unknown. All 20 tumours showed unmethylated promoter 4; UPD, uniparental disomy; loss chr 11, loss of chromosome 11or 11p15; LOI, loss of imprinting. [a]Age in months. [b]Chemo, chemotherapy before surgery; +6, –1 indicates that six and one tumours were treated and untreated, respectively, with chemotherapy before surgery. [c]%methyl CTCF6 indicates % methylated CTCF6 allele. [d]Results of SNP array. [e]Homo, homozygosity at *ApaI/AvaII* site; hetero, heterozygosity. [f]Results of SNP array analysis, methylation analysis of CTCF6 (m) and *ApaI/AvaII* polymorphism site analysis (p). [g]P1E, promoter 1-specific transcript. [h]P2M, the methylation status of promoter 2. [i]*CTNNB1* status: M, mutated; N, normal.

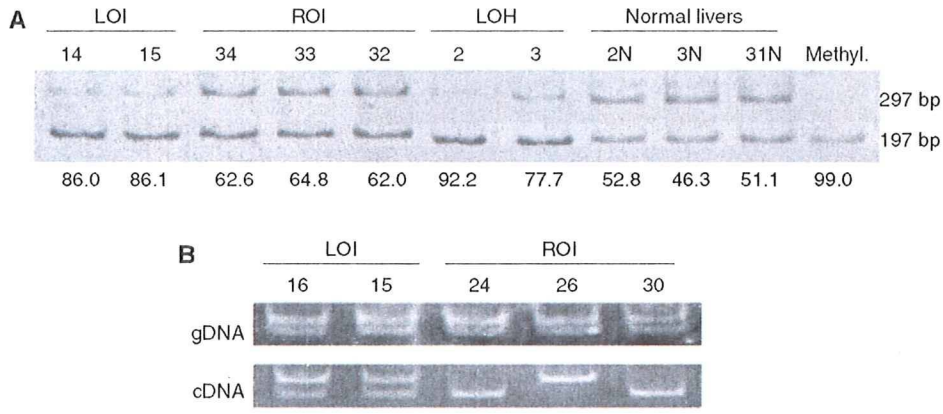

Figure 1 Analysis of *IGF2* alterations. (**A**) Examples of the methylation status of CTCF6 analysed by a combined bisulphite restriction assay (COBRA). Bisulphite-modified PCR products were digested with *Mlu*I. Upper and lower lanes indicate unmethylated and methylated fragments, respectively. Numbers above lanes indicate the tumour number. Numbers below lanes show the percentage of methylated DNA fragments containing CTCF6. The mean value of the DNA methylation percentages calculated from three COBRA experiments is shown in Table 1. Methyl., control methylated DNA. The *IGF2* status is shown above the tumour numbers. LOI, loss of *IGF2* imprinting; LOH, loss of heterozygosity in the *IGF2* region; ROI, retention of *IGF2* imprinting. (**B**) Electrophoretic pattern of genomic DNA PCR products or RT–PCR products after *Ava*II digestion. Reverse transcriptase–PCR analysis shows LOI in two tumours and ROI in three tumours.

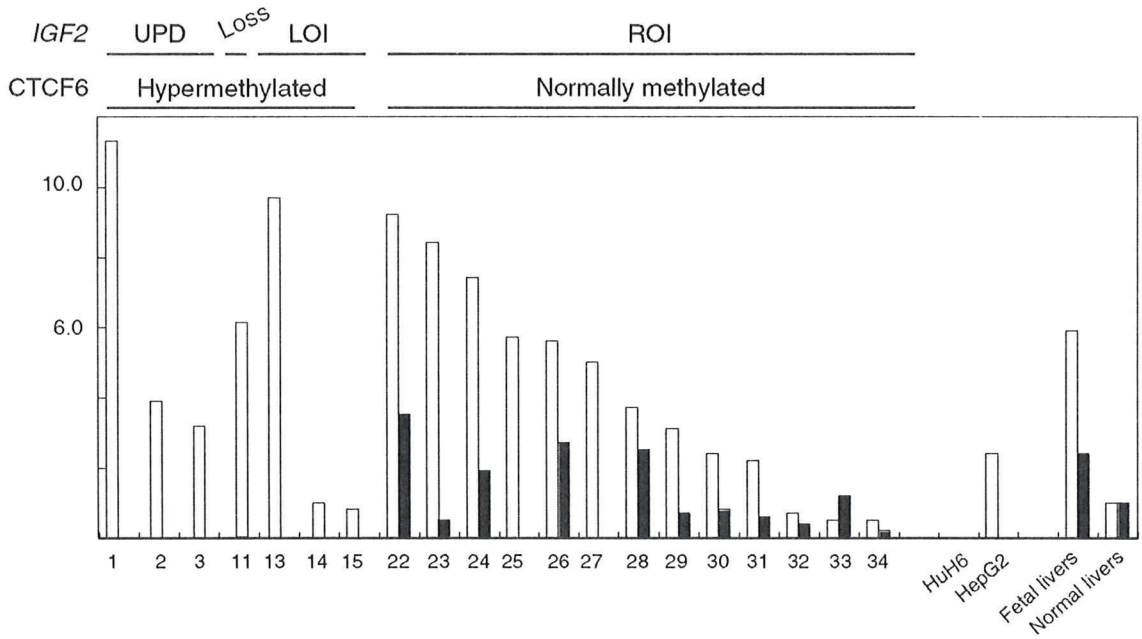

Figure 2 Results of quantitative real-time RT–PCR analysis of *IGF2* and *H19* mRNAs. Relative mRNA (*Y* axis) of total *IGF2* (open rectangles) and *H19* (closed rectangles) is plotted in 3 tumours with UPD, in 1 tumour with 11p15 loss, in 3 tumours with LOI, in 13 tumours with ROI, in 2 cell lines, in foetal liver total RNA and in adjacent normal liver tissues (a mean value of 3 samples). Tumours in each group are arranged in order by the levels of *IGF2* mRNA. Numbers below *X* axis indicate the tumour number shown in Table 1. *IGF2* status (UPD, loss of 11p15, LOI and ROI) and methylation status of CTCF6 at *H19* DMR (hypermethylated or normally methylated) are shown above the graph. Nine tumours (nos. 1–3, 11, 13–15, 25 and 27) and two cell lines expressed a minimal amount of *H19* mRNA, which was shown as zero in the graph. Similarly, HuH6 expressed a minimal amount of *IGF2* mRNA, which was shown as zero in the graph.

Incidences of tumours with *CTNNB1* mutation between any two groups of tumours classified on the basis of the *IGF2* status

DNA was available for *CTNNB1* mutation analysis in 48 of 54 HB tumours. The results are described in Table 1. There were no differences in the incidences of *CTNNB1* mutation between 7 tumours with *IGF2*-LOI and 29 tumours with *IGF2*-ROI or 12 tumours with *IGF2*-LOH, and between 29 tumours with *IGF2*-ROI and 12 tumours with *IGF2*-LOH.

DISCUSSION

In this study, biallelic and monoallelic *IGF2* expressions correlated with hypermethylation and normal methylation of CTCF6,

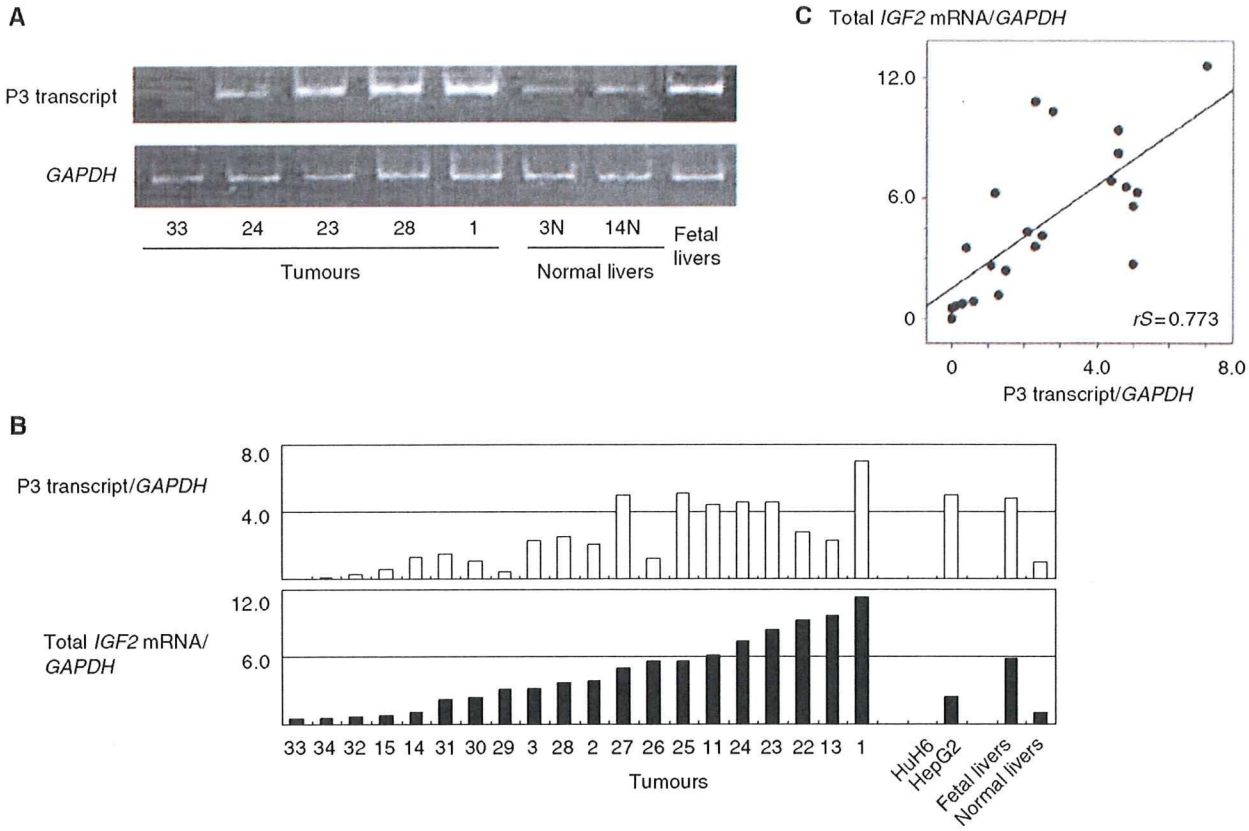

Figure 3 (**A**) Representative data of RT–PCR analysis of P3 transcripts. (**B**) Expression levels of P3 transcripts (upper lane) and total *IGF2* mRNA (lower lane) are plotted in 20 tumours, in 2 cell lines, in foetal liver tissues and normal liver tissues (a mean value of 3 samples). Tumours are arranged in order by total levels of *IGF2* mRNA. Numbers below *X* axis indicate the tumour number. (**C**) Correlation between levels of P3 transcript (*X* axis) and total *IGF2* mRNA (*Y* axis).

respectively, in two tumours with LOI and seven tumours with ROI (Table 1, Figure 1). In addition, the paternal origin of the duplicated *IGF2* loci was confirmed by the hypermethylated CTCF6 in 10 tumours with UPD. Furthermore, very low expression levels of *H19* mRNAs and substantial expression levels of *IGF2* mRNAs in HB tumours with UPD or LOI, and substantial expression levels of both *IGF2* and *H19* mRNA in HB tumours with ROI were found (Table 1 and Figure 2). Two (nos. 14 and 15) of three HB tumours with LOI expressed *IGF2* mRNA levels comparable to but not higher than those of *IGF2* mRNA in normal liver tissues. In addition, one cell line, HuH6, with LOI expressed minimal expression of *IGF2* mRNA, although Hartmann *et al* (2000) found the moderate expression in the same cell line. These findings may be explained by the speculation that such tumours expressed increased levels of *IGF2* mRNA at the critical time of tumorigenesis, but not at the time of surgical resection or after many passages of cell culture. From these findings, the hypothesis established for WT that the hypermethylation of maternal *H19* DMR causes LOI, and that LOI or duplication of paternal *IGF2* (UPD) results in overexpression of *IGF2*, may be also applied to HB.

Although the expression levels of *IGF2* mRNA were reported to be higher in WTs with UPD than in WTs with ROI in two series of WTs (Wang *et al*, 1996; Haruta *et al*, 2008), conflicting results were reported in *IGF2* mRNA levels between WTs with LOI and WTs with ROI (Wang *et al*, 1996; Ravenel *et al*, 2001). The present and earlier studies showed that all HB tumours with UPD and the majority of HB tumours with LOI or ROI expressed the higher levels of *IGF2* mRNA than normal liver tissues (Li *et al*, 1998b; Gray *et al*, 2000; Hartmann *et al*, 2000). This study also showed that P3 transcripts predominated in total *IGF2* mRNAs in HB tumours irrespective of the *IGF2* status (i.e., UPD, 11p15 loss, LOI or ROI); these findings were similar to those reported in foetal liver tissues showing elevated expression of *IGF2* mRNA with predominance of the P3 transcript (Li *et al*, 1998a). Thus, the high *IGF2* mRNA expression of many HB tumours with ROI may mimic the upregulation of *IGF2* expression in embryonic liver tissues, from which HB may arise.

In this study of 54 HB tumours, we found LOH in 12 (22.2%), LOI in 9 (16.7%) and ROI in 33 (61.1%). Hepatoblastoma tumours can be classified into those with LOH and those with ROH, and tumours with ROH can be further classified into those with LOI and those with ROI. For data comparison, the frequencies of LOH and LOI in the earlier and present series of HB tumours are shown in Tables 2 and 3, respectively (Davies, 1993; Montagna *et al*, 1994; Li *et al*, 1995; Rainier *et al*, 1995; Fukuzawa *et al*, 1999; Gray *et al*, 2000; Hartmann *et al*, 2000; Ross *et al*, 2000; Albrecht *et al*, 2004; Suzuki *et al*, 2008). Both frequencies of LOH and LOI were similar between the earlier and present series of HB tumours. When we compared the frequencies of LOH and LOI between HB and WT, the frequencies of LOH and LOI are lower in HB tumours than in WT tumours (Table 4). The present and earlier studies showed that levels of *IGF2* mRNA are higher in normal liver tissues than in normal kidney tissues, and in foetal liver tissues than in foetal kidney tissues, but showed similarly high levels in both WTs and HBs (part of the data not shown) (Hedborg *et al*, 1994; Haruta

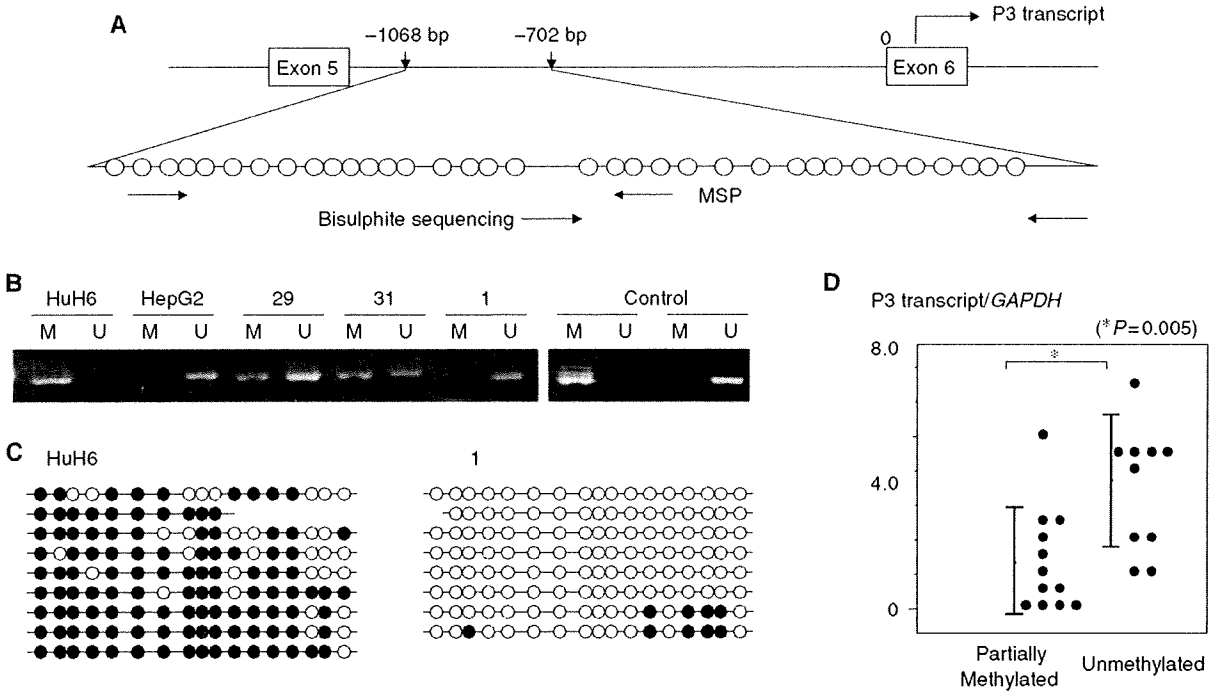

Figure 4 (**A**) Diagram of the *IGF2* P3 promoter region. Individual CpG dinucleotides located upstream of exon 6 (from −1068 to −702 bp) are represented by circles. Horizontal arrows indicate locations of PCR primers used for MSP and bisulphite sequencing. (**B**) Examples of the promoter methylation status using methylation-specific PCR. Polymerase chain reaction products of methylated or unmethylated P3 promoters from HB tumours are shown. Numbers above horizontal bars indicate the tumour number. M, methylated promoter; U, unmethylated promoter. (**C**) Bisulphite sequencing analysis of the methylation status of P3 promoter in HuH6 and one tumour (no. 1), which displayed complete methylation and complete unmethylation, respectively. Open and closed circles indicate unmethylated and methylated CpG dinucleotides, respectively. (**D**) Levels of P3 transcripts in tumours with partially methylated P3 promoter and tumours with unmethylated P3 promoter.

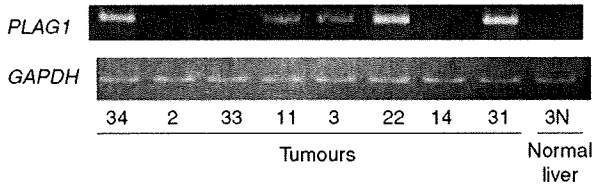

Figure 5 Representative data of RT–PCR analysis of *PLAG1* mRNA. Numbers below lanes indicate the tumour number.

et al, 2008), indicating that embryonal kidney tissues might be more susceptible to IGF2 stimulation than embryonal liver tissues. These findings might be related to higher incidences of UPD or LOI in WT than in HB.

The *IGF2* gene has four promoter regions and each promoter can initiate transcription producing a distinct *IGF2* transcript with different 5′-untranslated regions with a common translated region in the 3′-side (Li *et al*, 1998a). The *IGF2* gene is transcriptionally regulated in a development-dependent and tissue-specific manner. In the foetal liver, promoters P2, P3, and P4 are active and expressed monoallelically; P3 is the most active promoter and P1 is inactive. However, in the adult liver, P1 becomes dominant and is biallelically expressed, and P2, P3 and P4 activities are decreased or lost (Li *et al*, 1998a). In foetal liver tissues, P3 promoter methylation is inversely correlated with the P3 transcript expression. The inverse correlation between P3 promoter methylation and P3 transcript expression was reported earlier in seven HB tumours (Li *et al*, 1998b). This study confirmed the upregulation of P2, P3 and P4 transcripts and downregulation of P1 transcript, and

Table 2 Incidences of LOH of *IGF2* in previous and present series of hepatoblastoma and Wilms' tumours

References	Total number	LOH of *IGF2*[a]	No-LOH of *IGF2*	%
Hepatoblastoma				
Montagna *et al* (1994)	13	3	10	23.1
Fukuzawa *et al* (1999)	7	2	5	28.6
Gray *et al* (2000)	10	2	8	20.0
Hartmann *et al* (2000)	24	6	18	25.0
Albrecht *et al* (2004)	56	13	43	23.2
Suzuki *et al* (2008)	17	4	13	23.5
Total number	127	30	97	23.6
Present study	54	12	42	22.2
Wilms' tumour				
Grundy *et al* (1996)	260	93	167	35.8
Yuan *et al* (2005)	62	26	36	41.9

[a]Tumours with LOH of 11p15, but no informative *IGF2* locus are included.

the inverse correlation between P3 promoter methylation and P3 transcript expression in the majority of 20 HB tumours. Although P2, P3 and P4 transcripts were all correlated to the total amount of *IGF2* mRNAs, the earlier and present studies showed that the P3 transcript was most abundant and seemed to play a major role in the tumorigenesis of HB (Li *et al*, 1998b). Increased *IGF2* expression with the predominant P3 transcript was reported earlier in WTs with LOI or ROI (Vu and Hoffman, 1999). This study also showed that HB tumours with hypermethylated *H19* DMR tended to have an unmethylated P3 promoter, indicating that

Table 3 Incidences of LOI of *IGF2* in previous and present series of hepatoblastoma and Wilms' tumours

References	Total number[a]	LOI of *IGF2*	ROI of *IGF2*	%
Hepatoblastoma				
Davies (1993)	3	0	3	0
Montagna *et al* (1994)	5	1	4	20.0
Rainier *et al* (1995)	5	1	4	20.0
Li *et al* (1995)	3	1	2	33.3
Fukuzawa *et al* (1999)	4	1	3	25.0
Ross *et al* (2000)	13	3	10	23.1
Hartmann *et al* (2000)	5	3	2	60.0
Total number	38	10	28	26.3
Present study	42	9	33	21.4
Wilms' tumour				
Ravenel *et al* (2001)	36	15	21	41.7
Yuan *et al* (2005)	29	22	7	75.9

[a]Tumours with LOH of *IGF2* were excluded.

Table 4 Incidences of LOH, LOI and ROI of *IGF2* in hepatoblastoma and Wilms' tumours

References	Total number	LOH of *IGF2*	LOI of *IGF2*	ROI of *IGF2*
Hepatoblastoma				
Present study	54	12 (22.2%)	9 (16.7%)	33 (61.1%)
Wilms' tumour				
Fukuzawa *et al* (2004)	41	17 (41.5%)	13 (31.7%)	11 (26.8%)
Yuan *et al* (2005)	58	29 (50.0%)	22 (37.9%)	7 (12.1%)

the paternal P3 promoter or the maternal P3 promoter upstream of the aberrantly methylated *H19* DMR is likely to be unmethylated, probably because of stimulation of the enhancer signal. In contrast, the significance of unmethylation in the P3 promoter found in 4 (nos. 23, 24, 26 and 27) of 13 HB tumours with normally methylated *H19* DMR (ROI) remains unresolved.

PLAG1 located in 8q11 encodes a developmentally regulated transcription factor, and positively regulates *IGF2*. The P3 promoter region of *IGF2* contains *PLAG1* consensus-binding sites, and PLAG1 transactivates the transcription from embryonic *IGF2* promoter P3 in HB cell lines, HuH6 and HepG2 (Zatkova *et al*, 2004). *PLAG1* mRNA was highly expressed in most HB tumours compared with normal liver tissues. In this study, HB tumours with *PLAG1* mRNA expression showed and tended to show higher levels of P4 and P3 transcripts, respectively. Thus, the correlation of *PLAG1* mRNA expression with increased levels of P3 transcripts reported by Zatkova *et al* (2004) may be confirmed; furthermore, the correlation of *PLAG1* mRNA expression with increased levels of P4 transcripts was also suggested.

WTs can be classified at least into two groups; one has intralobar nephrogenic rest that is associated with *WT1* abnormality and the other has perilobar nephrogenic rest associated with *IGF2*-LOI (Ravenel *et al*, 2001). *CTNNB1* mutation is frequently found in WTs with *WT1* abnormality, but rare in WTs without *WT1* abnormality (Maiti *et al*, 2000). These findings suggest that WTs with no *WT1* abnormality may include a substantial number of tumours with *IGF2*-LOI, and that *CTNNB1* mutation and *IGF2*-LOI may be mutually exclusive in WT and also in HB. However, there were no differences in the incidences of *CTNNB1* mutation between HBs with *IGF2*-LOI and those with *IGF2*-ROI, or those with *IGF2*-LOH. We have recently reported a paper describing the occurrence of duplication of paternal *IGF2* or *IGF2*-LOI in half of WTs with *WT1* abnormalities (Haruta *et al*, 2008). Of two WTs with *IGF2*-LOI and *WT1* abnormality reported in that paper, one had *CTNNB1* mutation and the other had not. These findings suggest that *CTNNB1* mutation and *IGF2*-LOI may not be mutually exclusive in either WT or HB.

The IGF signalling pathway is activated in various cancers, and monoclonal antibodies targeting IGF1R have been recently developed; IGF1R is a transmembrane tyrosine kinase receptor, and both IGF1 and IGF2 are ligands for IGF1R (Foulstone *et al*, 2005). Early clinical trials using anti-IGF1R monoclonal antibodies showed promising results in refractory Ewing's sarcomas and rhabdomyosarcomas (Ryan and Goss, 2008). Because 20–30% of HB tumours do not respond to the current chemotherapy consisting of cisplatin and adriamycin (Perilongo *et al*, 2000; Fuchs *et al*, 2002), and the great majority of HB tumours overexpresses *IGF2*, as shown in the present and earlier studies, HB may be the next target tumour for antibody therapy.

ACKNOWLEDGEMENTS

This study was supported by Ministry of Health, Labor and Welfare, Japan for Third-Term Comprehensive Control Research for Cancer (Y Kaneko). We are grateful to Dr K Hiyama, Hiroshima University, a data administrator for JPLT, for data management. We also express our gratitude to the physicians participating in JPLT who supplied samples for this study.

REFERENCES

Albrecht S, Hartmann W, Houshdaran F, Koch A, Gärtner B, Prawitt D, Zabel BU, Russo P, Von Schweinitz D, Pietsch T (2004) Allelic loss but absence of mutations in the polyspecific transporter gene *BWR1A* on 11p15.5 in hepatoblastoma. *Int J Cancer* **111**: 627–632

Beeghly AC, Katsaros D, Wiley AL, Rigault de la Longrais IA, Prescott AT, Chen H, Puopolo M, Rutherford TJ, Yu H (2007) IGF-II promoter methylation and ovarian cancer prognosis. *J Cancer Res Clin Oncol* **133**: 713–723

Bell AC, Felsenfeld G (2000) Methylation of a CTCF-dependent boundary controls imprinted expression of the *Igf2* gene. *Nature* **405**: 482–485

Davies SM (1993) Maintenance of genomic imprinting at the IGF2 locus in hepatoblastoma. *Cancer Res* **53**: 4781–4783

Foulstone E, Prince S, Zaccheo O, Burns JL, Harper J, Jacobs C, Church D, Hassan AB (2005) Insulin-like growth factor ligands, receptors, and binding proteins in cancer. *J Pathol* **205**: 145–153

Fuchs J, Rydzynski J, Von Schweinitz D, Bode U, Hecker H, Weinel P, Bürger D, Harms D, Erttmann R, Oldhafer K, Mildenberger H (2002) Pretreatment prognostic factors and treatment results in children with hepatoblastoma. *Cancer* **95**: 172–182

Fukuzawa R, Breslow NE, Morison IM, Dwyer P, Kusafuka T, Kobayashi Y, Becroft DM, Beckwith JB, Perlman EJ, Reeve AE (2004) Epigenetic differences between Wilms' tumours in white and East-Asian children. *Lancet* **363**: 446–451

Fukuzawa R, Umezawa A, Ochi K, Urano F, Ikeda H, Hata J (1999) High frequency of inactivation of the imprinted *H19* gene in 'sporadic' hepatoblastoma. *Int J Cancer* **82**: 490–497

Gray SG, Eriksson T, Ekström C, Holm S, von Schweinitz D, Kogner P, Sandstedt B, Pietsch T, Ekström TJ (2000) Altered expression of members of the IGF-axis in hepatoblastomas. *Br J Cancer* **82**: 1561–1567

Grundy P, Telzerow P, Moksness J, Breslow NE (1996) Clinicopathologic correlates of loss of heterozygosity in Wilms' tumors: a preliminary analysis. *Med Pediatr Oncol* **27**: 429–433

Hark AT, Schoenherr CJ, Katz DJ, Ingram RS, Levorse JM, Tilghman SM (2000) CTCF mediates methylation-sensitive enhancer-blocking activity at the *H19/Igf2* locus. *Nature* **405:** 486–489

Hartmann W, Waha A, Koch A, Goodyer CG, Albrecht S, von Schweinitz D, Pietsch T (2000) $p57^{KIP2}$ is not mutated in hepatoblastoma but shows increased transcriptional activity in a comparative analysis of the three imprinted genes $p57^{KIP2}$, *IGF2*, and *H19*. *Am J Pathol* **157:** 1393–1403

Haruta M, Arai Y, Sugawara W, Watanabe N, Honda S, Ohshima J, Soejima H, Nakadate H, Okita H, Hata J, Fukuzawa M, Kaneko Y (2008) Duplication of paternal *IGF2* or loss of maternal *IGF2* imprinting occurs in half of Wilms tumors with various structural *WT1* abnormalities. *Genes Chromosomes Cancer* **47:** 712–727

Hedborg F, Holmgren L, Sandstedt B, Ohlsson R (1994) The cell type-specific *IGF2* expression during early human development correlates to the pattern of overgrowth and neoplasia in the Beckwith–Wiedemann syndrome. *Am J Pathol* **145:** 802–817

Herman JG, Graff JR, Myöhänen S, Nelkin BD, Baylin SB (1996) Methylation-specific PCR: a novel PCR assay for methylation status of CpG islands. *Proc Natl Acad Sci USA* **93:** 9821–9826

Honda S, Haruta M, Sugawara W, Sasaki F, Ohira M, Matsunaga T, Yamaoka H, Horie H, Ohnuma N, Nakagawara A, Hiyama E, Todo S, Kaneko Y (2008) The methylation status of *RASSF1A* promoter predicts responsiveness to chemotherapy and eventual cure in hepatoblastoma patients. *Int J Cancer* **123:** 1117–1125

Koch A, Denkhaus D, Albrecht S, Leuschner I, Von Schweinitz D, Pietsch T (1999) Childhood hepatoblastomas frequently carry a mutated degradation targeting box of the β-catenin gene. *Cancer Res* **59:** 269–273

Li X, Adam G, Cui H, Sandstedt B, Ohlsson R, Ekström TJ (1995) Expression, promoter usage and parental imprinting status of insulin-like growth factor II (*IGF2*) in human hepatoblastoma: uncoupling of *IGF2* and *H19* imprinting. *Oncogene* **11:** 221–229

Li X, Gray SG, Flam F, Pietsch T, Ekström TJ (1998a) Developmental-dependent DNA methylation of the *IGF2* and *H19* promoters is correlated to the promoter activities in human liver development. *Int J Dev Biol* **42:** 687–693

Li X, Kogner P, Sandstedt B, Haas OA, Ekström TJ (1998b) Promoter-specific methylation and expression alterations of *igf2* and *h19* are involved in human hepatoblastoma. *Int J Cancer* **75:** 176–180

Lu L, Katsaros D, Wiley A, Rigault de la Longrais IA, Puopolo M, Schwartz P, Yu H (2006) Promoter-specific transcription of insulin-like growth factor II in epithelial ovarian cancer. *Gynecol Oncol* **103:** 990–995

Maiti S, Alam R, Amos CI, Huff V (2000) Frequent association of *β-catenin* and *WT1* mutations in Wilms tumors. *Cancer Res* **60:** 6288–6292

Matsunaga T, Sasaki F, Ohira M, Hashizume K, Hayashi A, Hayashi Y, Matsuyama K, Mugishima H, Ohnuma N (2004) The role of surgery in the multimodal treatment for hepatoblastomas. *Shounigan* **41:** 205–210 (in Japanese)

Montagna M, Menin C, Chieco-Bianchi L, D'Andrea E (1994) Occasional loss of constitutive heterozygosity at 11p15.5 and imprinting relaxation of the *IGFII* maternal allele in hepatoblastoma. *J Cancer Res Clin Oncol* **120:** 732–736

Perilongo G, Shafford EA (1999) Liver tumours. *Eur J Cancer* **35:** 953–958

Perilongo G, Shafford S, Plaschkes J (2000) SIOPEL trials using preoperative chemotherapy in hepatoblastoma. *Lancet Oncol* **1:** 94–100

Rainier S, Dobry CJ, Feinberg AP (1995) Loss of imprinting in hepatoblastoma. *Cancer Res* **55:** 1836–1838

Ravenel JD, Broman KW, Perlman EJ, Niemitz EL, Jayawardena TM, Bell DW, Haber DA, Uejima H, Feinberg AP (2001) Loss of imprinting of insulin-like growth factor-II (IGF2) gene in distinguishing specific biologic subtypes of Wilms tumor. *J Natl Cancer Inst* **93:** 1698–1703

Ross JA, Radloff GA, Davies SM (2000) *H19* and *IGF-2* allele-specific expression in hepatoblastoma. *Br J Cancer* **82:** 753–756

Ryan PD, Goss PE (2008) The emerging role of the insulin-like growth factor pathway as a therapeutic target in cancer. *Oncologist* **13:** 16–24

Satoh Y, Nakagawachi T, Nakadate H, Kaneko Y, Masaki Z, Mukai T, Soejima H (2003) Significant reduction of *WT1* gene expression, possibly due to epigenetic alteration in Wilms' tumor. *J Biochem* **133:** 303–308

Steenman MJ, Rainier S, Dobry CJ, Grundy P, Horon IL, Feinberg AP (1994) Loss of imprinting of *IGF2* is linked to reduced expression and abnormal methylation of *H19* in Wilms tumor. *Nat Genet* **7:** 433–439

Sugawara W, Haruta M, Sasaki F, Watanabe N, Tsunematsu Y, Kikuta A, Kaneko Y (2007) Promoter hypermethylation of the *RASSF1A* gene predicts the poor outcome of patients with hepatoblastoma. *Pediatr Blood Cancer* **49:** 240–249

Suzuki M, Kato M, Yuyan C, Takita J, Sanada M, Nannya Y, Yamamoto G, Takahashi A, Ikeda H, Kuwano H, Ogawa S, Hayashi Y (2008) Whole-genome profiling of chromosomal aberrations in hepatoblastoma using high-density single-nucleotide polymorphism genotyping microarrays. *Cancer Sci* **99:** 564–570

Takai D, Gonzales FA, Tsai YC, Thayer MJ, Jones PA (2001) Large scale mapping of methylcytosines in CTCF-binding sites in the human *H19* promoter and aberrant hypomethylation in human bladder cancer. *Hum Mol Genet* **10:** 2619–2626

Taniguchi K, Roberts LR, Aderca IN, Dong X, Qian C, Murphy LM, Nagorney DM, Burgart LJ, Roche PC, Smith DI, Ross JA, Liu W (2002) Mutational spectrum of beta-catenin, *AXIN1*, and *AXIN2* in hepatocellular carcinomas and hepatoblastomas. *Oncogene* **21:** 4863–4871

Toretsky JA, Helman LJ (1996) Involvement of IGF-II in human cancer. *J Endocrinol* **149:** 367–372

Vu TH, Hoffman AR (1999) Alterations in the promoter-specific imprinting of insulin-like growth factor-II gene in Wilms tumor. *J Biol Chem* **271:** 9014–9023

Wang WH, Duan JX, Vu TH, Hoffman AR (1996) Increased expression of the insulin-like growth factor-II gene in Wilms' tumor is not dependent on loss of genomic imprinting or loss of heterozygosity. *J Biol Chem* **271:** 27863–27870

Watanabe N, Haruta M, Soejima H, Fukushi D, Yokomori K, Nakadate H, Okita H, Hata J, Fukuzawa M, Kaneko Y (2007) Duplication of the paternal *IGF2* allele in trisomy 11 and elevated expression levels of *IGF2* mRNA in congenital mesoblastic nephroma of the cellular or mixed type. *Genes Chromosomes Cancer* **46:** 929–935

Watanabe N, Nakadate H, Haruta M, Sugawara W, Sasaki F, Tsunematsu Y, Kikuta A, Fukuzawa M, Okita H, Hata J, Soejima H, Kaneko Y (2006) Association of 11q loss, trisomy 12, and possible 16q loss with loss of imprinting of insulin-like growth factor-II in Wilms tumor. *Genes Chromosomes Cancer* **45:** 592–601

Yuan E, Li CM, Yamashiro DJ, Kandel J, Thaker H, Murty VV, Tycko B (2005) Genomic profiling maps loss of heterozygosity and defines the timing and stage dependence of epigenetic and genetic events in Wilms' tumors. *Mol Cancer Res* **3:** 493–502

Zatkova A, Rouillard JM, Hartmann W, Lamb BJ, Kuick R, Eckart M, von Schweinitz D, Koch A, Fonatsch C, Pietsch T, Hanash SM, Wimmer K (2004) Amplification and overexpression of the *IGF2* regulator *PLAG1* in hepatoblastoma. *Genes Chromosomes Cancer* **39:** 126–137

Int. J. Cancer: **123,** 2087–2094 (2008)

Expression of *TSLC1*, a candidate tumor suppressor gene mapped to chromosome 11q23, is downregulated in unfavorable neuroblastoma without promoter hypermethylation

Kiyohiro Ando[1], Miki Ohira[1], Toshinori Ozaki[1], Atsuko Nakagawa[2], Kohei Akazawa[3], Yusuke Suenaga[1], Yohko Nakamura[1], Tadayuki Koda[4], Takehiko Kamijo[1], Yoshinori Murakami[5] and Akira Nakagawara[1]*

[1]*Division of Biochemistry, Chiba Cancer Center Research Institute, Chiba, Japan*
[2]*Division of Clinical Laboratory, National Center for Child Health and Development, Tokyo, Japan*
[3]*Division of Medical Information, Niigata University Medical and Dental Hospital, Niigata, Japan*
[4]*Center for Functional Genomics, Hisamitsu Pharmaceutical Co. Inc., Chiba, Japan*
[5]*Division of Molecular Pathology, Department of Cancer Biology, Institute of Medical Science, The University of Tokyo, Tokyo, Japan*

Although it has been well documented that loss of human chromosome 11q is frequently observed in primary neuroblastomas, the smallest region of overlap (SRO) has not yet been precisely identified. Previously, we performed array-comparative genomic hybridization (array-CGH) analysis for 236 primary neuroblastomas to search for genomic aberrations with high-resolution. In our study, we have identified the SRO of deletion (10-Mb or less) at 11q23. Within this region, there exists a *TSLC1/IGSF4/CADM1* gene (*Tumor suppressor in lung cancer 1/Immunoglobulin superfamily 4/Cell adhesion molecule 1*), which has been identified as a putative tumor suppressor gene for lung and some other cancers. Consistent with previous observations, we have found that 35% of primary neuroblastomas harbor loss of heterozygosity (LOH) on *TSLC1* locus. In contrast to other cancers, we could not detect the hypermethylation in its promoter region in primary neuroblastomas as well as neuroblastoma-derived cell lines. The clinicopathological analysis demonstrated that *TSLC1* expression levels significantly correlate with stage, Shimada's pathological classification, *MYCN* amplification status, *TrkA* expression levels and DNA index in primary neuroblastomas. The immunohistochemical analysis showed that TSLC1 is remarkably reduced in unfavorable neuroblastomas. Furthermore, decreased expression levels of *TSLC1* were significantly associated with a poor prognosis in 108 patients with neuroblastoma. Additionally, TSLC1 reduced cell proliferation in human neuroblastoma SH-SY5Y cells. Collectively, our present findings suggest that *TSLC1* acts as a candidate tumor suppressor gene for neuroblastoma.

Key words: *TSLC1/IGSF4/CADM1*; neuroblastoma; 11q23; tumor suppressor

Neuroblastoma is one of the most common solid tumors in childhood and originates from the sympathoadrenal lineage of neural crest. Its biological as well as clinical behavior is highly heterogeneous in different prognostic subsets. Tumors found in patients under 1 year of age often regress spontaneously or differentiate and result in a favorable prognosis.[1] In a sharp contrast to these favorable neuroblastomas, tumors found in patients over 1 year of age are often aggressive with an unfavorable prognosis despite an intensive therapy. A large number of multiple genomic aberrations including DNA index, *MYCN* amplification status, allelic loss of the distal part of chromosome 1p and the gain of chromosome 17q have been identified in neuroblastoma.[2,3]

Alternatively, allelic loss of 11q has been frequently observed in advanced stage of neuroblastoma with single copy of *MYCN*. Indeed, 30% of tumors harbor allelic loss of 11q, and it might be an independent prognostic indicator for clinically high-risk patients without *MYCN* amplification.[4,5] Aberrant deletions of 11q often occur in a distal part of its long arm. Although several lines of evidence delineated the smallest region of overlaps (SRO) of deletions at 11q, it remains unclear whether there could exist a candidate tumor suppressor gene(s) implicated in biological and clinical behaviors of neuroblastoma.[6,7] Recently, we have performed an array-comparative genomic hybridization (array-CGH) analysis using 236 primary neuroblastomas and finally defined the SRO (10-Mb or less) at 11q23.[3,8] During our extensive search for the already identified candidate tumor suppressor gene(s) within this region, we have found that *TSLC1/IGSF4/CADM1* gene is localized within this region.

TSLC1 gene has been originally identified as a putative tumor suppressor for non-small-cell lung cancer (NSCLC) located at chromosome 11q23 by functional complementation strategy of a human lung cancer cell line. The downregulation of *TSLC1* gene was frequently detected in various human cancers including NSCLC, prostate cancers, hepatocellular carcinomas and pancreatic cancers through its allelic loss as well as hypermethylation of its promoter region. In spite of an extensive mutation search, only 2 inactivating *TSLC1* gene mutations were detected in 161 primary tumors and tumor-derived cell lines, suggesting that *TSLC1* is rarely mutated in human cancers.[9] *TSLC1* encodes a single membrane-spanning glycoprotein involved in cell–cell adhesion through homophilic trans interaction.[10] Accumulating evidence indicates that TSLC1 is significantly associated with biological aggressiveness and metastasis of certain types of cancer,[11–16] whereas the functional significance of TSLC1 in neuroblastoma remains elusive.

In the present study, we have further delineated the SRO of 11q deletion in primary neuroblastoma by array-CGH analysis and finally identified *TSLC1* gene within this region. In contrast to the other cancers, hypermethylation of *TSLC1* promoter region was undetectable in neuroblastoma. Intriguingly, the expression levels of *TSLC1* gene were highly associated with clinical stage, Shimada's pathological classification, *MYCN* amplification status, *TrkA* expression levels and DNA index in primary neuroblastoma.

Additional Supporting Information may be found in the online version of this article.

Abbreviations: array-CGH, array-comparative genomic hybridization; BAC, bacterial artificial chromosome; LOH, loss of heterozygosity; PARP, poly(ADP-ribose) polymerase; SRO, smallest region of overlap; STS, sequence-tagged-site; TSA, trichostatin A; TSLC1, tumor suppressor in lung cancer 1.

Grant sponsors: Ministry of Health, Labour and Welfare for Third Term Comprehensive Control Research for Cancer; Ministry of Education, Culture, Sports, Science and Technology, Japan; Scientific Research from Japan Society for the Promotion of Science.

***Correspondence to:** Chiba Cancer Center Research Institute, 666-2 Nitona, Chuo-ku, Chiba 260-8717. Fax: +81-43-265-4459.
E-mail: akiranak@chiba-cc.jp

Received 21 February 2008; Accepted after revision 19 May 2008
DOI 10.1002/ijc.23776
Published online 22 August 2008 in Wiley InterScience (www.interscience.wiley.com).

Material and methods

Patients, tumor specimens and cell lines

One hundred and eight tumor specimens used in the present study were kindly provided from various institutions and hospitals in Japan (see Supplementary Information). Informed consent was obtained at each institution or hospital. All tumors were diagnosed clinically as well as pathologically as neuroblastoma and staged according to the International Neuroblastoma Staging System (INSS) criteria.[17] Twenty-seven patients were Stage 1, 15 Stage 2, 36 Stage 3, 23 Stage 4 and 7 Stage 4S. The patients were treated by the standard protocols as described previously.[18,19] *MYCN* copy number, *TrkA* mRNA expression levels and DNA index were measured as reported previously.[20] Our present study was approved by the Institutional Review Board of the Chiba Cancer Center (CCC7817).

Human tumor-derived cell lines were cultured in RPMI 1640 medium (Nissui, Tokyo, Japan) supplemented with 10% heat-inactivated fetal bovine serum (FBS, Invitrogen, Carlsbad, CA) and 50 μg/ml penicillin/streptomycin (Invitrogen) in an incubator with humidified air at 37°C with 5% CO_2.

Array-comparative genomic hybridization

Array-CGH analysis was performed using UCSF BAC array (2464 BACs, ≈1 Mb resolution) with 236 primary neuroblastomas. Detailed experimental procedures and the criteria for losses and gains were described previously.[3,20–22]

LOH analysis

Genomic DNA prepared from neuroblastomas and bloods was amplified by PCR-based strategy using the primer set, one of which was labeled with fluorescent dye CY5. The amplified fragments including 3 polymorphic STS markers encompassing *TSLC1*, *D11S4111*, *D11S2077* and *D11S1885*, were separated by 6% polyacrylamide gels containing 6 M urea using an automated ALF express DNA sequencer.

Semiquantitative and quantitative reverse transcription-PCR analysis

Total RNA was prepared from the indicated primary neuroblastomas, various human normal tissues and tumor-derived cell lines were subjected to semiquantitative RT-PCR using SuperScript II reverse transcriptase and random primers (Invitrogen), according to the manufacturer's instructions. Oligonucleotide primer set used to amplify *TSLC1* by semiquantitative RT-PCR was as follows: 5′-CATTTTGGAATTTGCCTGCT-3′ (sense) and 5′-GGCAGCAG-CAAAGAG TTTTC-3′ (antisense). Quantitative real-time PCR was carried out using TaqMan(R) Gene Expression Assay System (Applied Biosystems, Foster City, CA) as described previously.[20] In brief, expression levels were calculated as a ratio of mRNA level for a given gene relative to mRNA for *GAPDH* in the same cDNA. The oligonucleotide primers and TaqMan probes, labeled at the 5′-end with the reporter dye 6-carboxyfluorescein (FAM) and at the 3′-end with 6-carboxytetramethylrhodamine (TAMRA), were provided by Applied Biosystems (Hs00942508_m1).

Immunohistochemistry

A 4-μm-thick section of formalin-fixed, paraffin-embedded tissues were stained with hematoxylin and eosin and the adjacent sections were immunostained for TSLC1 using polyclonal anti-TSLC1 antibody (CC2) as described previously.[10] The BenchMark XT immunostainer (Ventana Medical Systems, Tucson, AZ) and 3-3′ diaminobenzidine detection kit (Ventana Medical Systems) were used to visualize TSLC1. Appropriate positive and negative control experiments were also performed in parallel for each immunostaining.

Small interfering RNA

TSLC1 siRNA (GUCAAUAAGAGUGACGACUUU) and Stealth RNAi Negative Control Duplex were purchased from Sigma-Aldrich (St. Louis, MO) and Invitrogen, respectively.

Transfection

Neuroblastoma-derived SH-SY5Y cells were transfected with the indicated combinations of expression plasmids or with siRNA against TSLC1 using LipofectAMINE 2000 or LipofectAMINE RNAiMAX transfection reagent (Invitrogen), according to the manufacturer's recommendations.

Colony formation assay

SH-SY5Y and SK-N-AS cells (1×10^5 cells/plate) were seeded in 6-well cell culture plates and transfected with or without the increasing amounts of the expression plasmid for TSLC1 (0, 250, 750 or 1,000 ng). Total amounts of plasmid DNA per transfection were kept constant (1 μg) with the empty plasmid (pcDNA3.1-Hygro (+); Invitrogen). Forty-eight hours after transfection, cells were transferred into the fresh medium containing hygromycin (at a final concentration of 200 μg/ml) and maintained for 14 days. Drug-resistant colonies were then stained with Giemsa's solution and numbers of drug-resistant colonies were scored.

Cell growth assay

SH-SY5Y cells (6×10^5 cells/dish) were seeded in 10-cm diameter cell culture dish and transiently transfected with siRNA against TSLC1 (240 pmol). Thirty-six hours after transfection, 2×10^4 cells were transferred into 6-well plates and transfected with 60 pmol of siRNA against TSLC1. At the indicated time points after transfection, number of viable cells was measured using a Coulter Counter (Coulter Electronics, Hialeah, Finland).

Bisulfite-sequencing

Sodium bisulfite-mediated modification of genomic DNA was performed using BisulFast Methylated DNA Detection Kit (Toyobo, Osaka, Japan), according to the manufacture's instructions. Modified genomic DNA was subjected to PCR-based amplification with a primer set as described previously.[23] The PCR products containing the promoter region of *TSLC1* gene were purified by PCR Purification Kit (Qiagen, Valencia, CA) and their nucleotide sequences were determined by using a 3730 DNA Analyzer (Applied Biosystem).

Statistical analysis

Fisher's exact tests were employed to examine possible associations between *TSLC1* expression and other prognostic indicators such as age. The difference between high and low expression levels of *TSLC1* was based on the mean value obtained from quantitative real-time PCR analysis. Kaplan-Meier survival curves were calculated, and survival distributions were compared using the log-rank test. Cox regression models were used to investigate the associations between *TSLC1* expression levels, age, *MYCN* amplification status, INSS and survival. Differences were considered significant if the p-value was less than 0.05.

Results

Array-comparative genomic hybridization analysis identifies the smallest region of overlaps of deletion in neuroblastoma at 11q23

We have previously performed array-CGH analysis using UCSF BAC array (2464 BACs, ≈1-Mb resolution) and 236 primary neuroblastomas.[3] In our array-CGH study, 66 tumors were revealed to have partial deletion of 11q as shown in Figure 1*a*, whose SRO were approximately 10-Mb long at 11q23 (from physical location of 110,979 to 119,806 kb in UCSC database, May 2006). To date, the data base analysis demonstrated that there could exist approximately 100 genes within this region. Of inter-

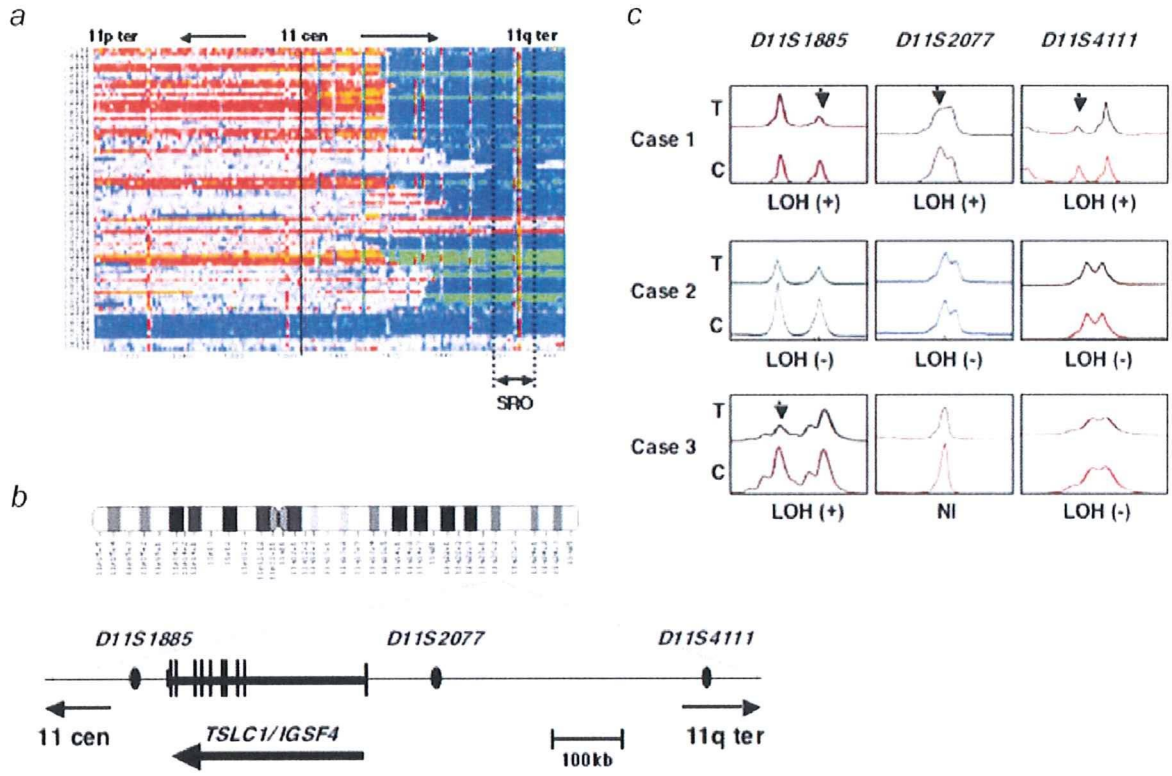

FIGURE 1 – Identification of the SRO of deletion at 11q in primary neuroblastoma. (*a*) Array-CGH analysis. Blue color indicates the position of the deleted area in each case. The smallest region of overlaps (SRO) of deletion at 11q is also shown. (*b*) The schematic drawing of the relative positions of 3 independent polymorphic markers at 11q23 used in the present study and *TSLC1* gene on human chromosome 11. (*c*) Representative electropherograms obtained from LOH analysis. Genomic DNA prepared from primary tumors (T) and their corresponding blood (C) was subjected to LOH analysis. Allelic losses are indicated by arrowheads. NI, not informative.

est, *TSLC1* gene which has been considered as a putative tumor suppressor for human lung as well as other cancers[9] locates within this region (Fig. 1*b*). These observations prompted us to perform loss of heterozygosity (LOH) as well as expression studies of *TSLC1* gene in primary neuroblastoma.

LOH at the TSLC1 locus is frequently detected in primary neuroblastoma

According to the previous observations,[9,24] tumor-specific downregulation of *TSLC1* gene might be largely attributed to loss of one allele in association with the hypermethylation of its promoter region in the remaining allele. To address whether LOH of *TSLC1* locus could be frequently detectable in primary neuroblastoma, we carried out LOH analysis using 3 independent fluorescently labeled polymorphic microsatellite markers (*D11S1885*, *D11S2077* and *D11S4111*) surrounding *TSLC1* gene (Fig. 1*b*). In accordance with the previous results,[9,25,26] the incidence of 11q23 LOH was 22% (7 of 32) and 45% (18 of 40) in favorable neuroblastomas (Stage 1 or 2) and unfavorable ones (Stage 3 or 4), respectively (data not shown). Statistical Fisher's exact test analysis revealed that the presence of LOH at this locus is associated with unfavorable neuroblastomas ($p = 0.0493$; data not shown). It is worth noting that LOH is detectable at *D11S1885* but not at *D11S4111* in Case 3 tumor (Fig. 1*c*), indicating that a putative chromosome breakpoint might exist between these loci.

Downregulation of TSLC1 expression is frequently observed in unfavorable neuroblastomas

Based on the previous observations,[11–16] the expression levels of *TSLC1* were significantly reduced in advanced stages of tumors as compared with those in early stages of tumors. We then examined the expression levels of *TSLC1* in 16 favorable neuroblastomas without *MYCN* amplification and 16 unfavorable ones with *MYCN* amplification. As clearly shown in Figure 2*a*, *TSLC1* was expressed at lower levels in unfavorable neuroblastomas relative to favorable ones as examined by semiquantitative RT-PCR. To ask whether there could exist a possible relationship between downregulation of *TSLC1* and *MYCN* amplification, we examined the expression levels of *TSLC1* in various neuroblastoma-derived cell lines bearing single copy of *MYCN* or *MYCN* amplification. As shown in Supplementary Figure 1*a*, a significant downregulation of *TSLC1* expression was detected in 2 of 6 neuroblastoma cell lines carrying single copy of *MYCN* (OAN and CNB-RT) and in 4 of 21 (CHP134, KP-N-NS, SK-N-DZ and NMB) bearing *MYCN* amplification as examined by semiquantitative RT-PCR. In addition, there was no obvious correlation between the expression levels of *TSLC1* and loss of 11q except OAN, SK-N-DZ and NMB. Next, we checked the expression levels of *TSLC1* in various human adult and fetal tissues. As seen in Supplementary Figure 1*b*, *TSLC1* was highly expressed in normal neuronal tissues, adrenal gland, testis, prostate and liver. Our present results suggest that *TSLC1* is expressed in normal neuronal tissues and its expression levels might be regulated in a *MYCN*-dependent manner in

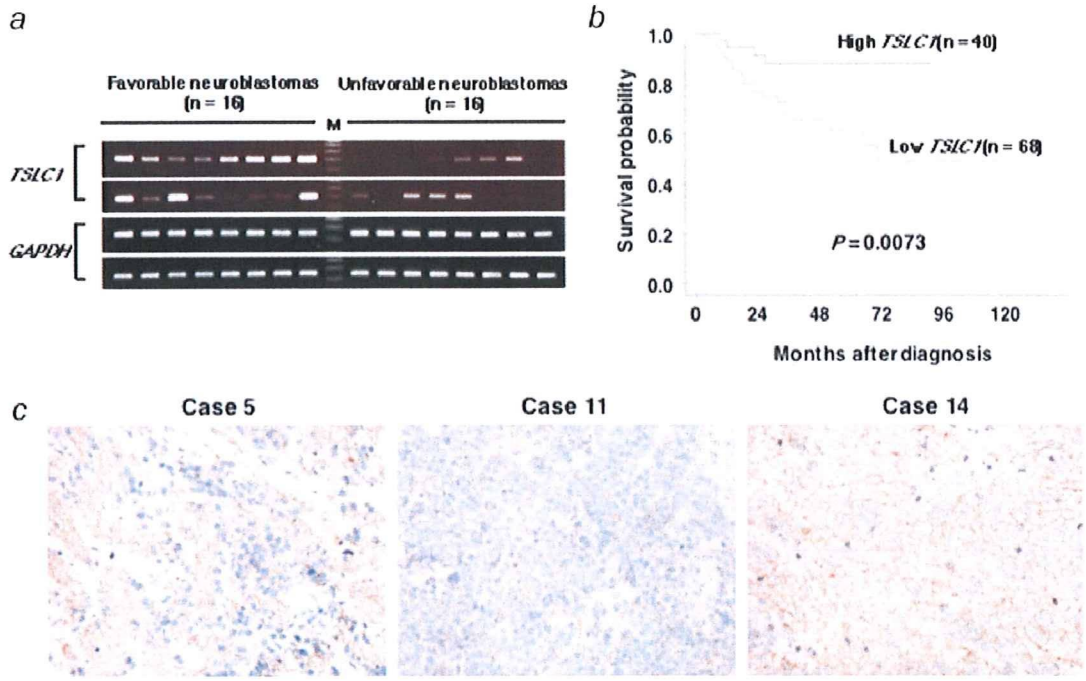

FIGURE 2 – Expression levels of *TSLC1* in primary neuroblastomas. (*a*) Expression of *TSLC1* in 16 favorable neuroblastomas bearing single copy of *MYCN* (Stage 1, higher expression levels of *TrkA*) and 16 unfavorable ones carrying *MYCN* amplification (stages 3 and 4, lower expression levels of *TrkA*). Total RNA was prepared from the indicated neuroblastoma tissues, reverse transcribed and amplified by PCR to examine the expression levels of *TSLC1*. *GAPDH* serves as an internal control. (*b*) Kaplan-Meier survival curves of patients with neuroblastomas based on higher or lower expression levels of *TSLC1*. Expression levels of *TSLC1* in 108 primary neuroblastoma samples categorized by their clinical stage were examined by a quantitative real-time PCR. Relative expression levels of *TSLC1* mRNA were determined by calculating the ratio between *GAPDH* and *TSLC1*. (*c*) Immunohistochemical analysis. Tumor samples derived from Case 5 (favorable neuroblastoma bearing single copy of *MYCN*), Case 11 (unfavorable neuroblastoma with *MYCN* amplification) and Case 14 (unfavorable neuroblastoma carrying single copy of *MYCN*) were fixed and stained with polyclonal anti-TSLC1 antibody.

primary neuroblastoma but not in neuroblastoma-derived cell lines.

Lower expression levels of TSLC1 are associated with poor outcome of neuroblastoma

To evaluate whether there could exist a possible relationship between *TSLC1* expression levels and clinicopathological factors of neuroblastoma patients, we have performed a quantitative real-time PCR. For this purpose, total RNA prepared from 108 primary neuroblastoma samples was subjected to a quantitative real-time PCR. According to the mean values of its expression levels obtained from a quantitative real-time PCR, these patients were divided into 2 groups including 40 patients with tumors expressing higher levels of *TSLC1* (High *TSLC1*) and 68 patients with tumors expressing lower levels of *TSLC1* (Low *TSLC1*). As shown in Table I, the significant differences were detectable between the above-mentioned 2 groups with respect to INSS stage, Shimada's pathological classification, copy number of *MYCN*, *TrkA* expression levels and DNA index. In contrast, no significant differences were observed between them with respect to their age, tumor origin and LOH on *TSLC1* locus.

We then examined whether there could exist a possible correlation between the expression levels of *TSLC1* in primary neuroblastomas and the survival of patients with neuroblastomas. The log-rank test showed that lower expression levels of *TSLC1* significantly correlate with unfavorable outcome ($p = 0.007$) as shown

TABLE I – CORRELATION BETWEEN *TSLC1* EXPRESSION AND OTHER PROGNOSTIC FACTORS OF NEUROBLASTOMA

Terms	*TSLC1* expression		*p*-Value
	High *TSLC1* ($n = 40$)	Low *TSLC1* ($n = 68$)	
Age (year)			
<1.5	23	29	
>1.5	17	39	0.1646
Tumor origin			
Adrenal grand	20	36	
Others	20	30	0.6915
Stage			
1, 2, 4S	24	25	
3, 4	16	43	0.0274
Shimada pathology			
Favorable	31	35	
Unfavorable	6	22	0.0227
MYCN copy number			
Single	38	51	
Amplified	2	17	0.0086
TrkA expression			
High	28	28	
Low	12	37	0.0090
DNA index			
Diploidy	8	39	
Aneuploidy	28	19	<0.0001
LOH			
(−)	18	29	
(+)	9	16	>0.9999

TABLE II – IMMUNOHISTOCHEMICAL ANALYSIS OF *TSLC1* EXPRESSION IN PRIMARY NEUROBLASTOMAS

Case	Age/Gender	*MYCN*	INPC	Primary site	Stage (INSS)	TSLC1
4	6 m/M	NA	NBL, Poorly diff., Low MKI, FH	Mediastinum	Stage 1	(+)
5	7 m/M	NA	NBL, Poorly diff., Low MKI, FH	Adrenal	Stage 1	(+)
6	9 m/M	NA	NBL, Poorly diff., Low MKI, FH	Adrenal	Stage 1	(+)
7	25 m/M	NA	NBL, Differentiating, Low MKI, FH	Adrenal	Stage 4	(+)
8	29 m/M	NA	NBL, Differentiating, Low MKI, FH	Mediastinum	Stage 2	(+)
9	13 m/M	A	NBL, Poorly diff., High MKI, UH	Adrenal	Stage 4	(−)
10	13 m/M	A	NBL, Poorly diff., Low MKI, UH	Abdominal	Stage 4	(−)
11	18 m/M	A	NBL, Poorly diff., Low MKI, UH	Adrenal	Stage 3	(−)
12	8 y/M	NA	NBL, Poorly diff., Low MKI, UH	Adrenal	Stage 4	(+)
13	8 m/M	NA	nGNB (NBL, poorly diff., Low MKI), UH	Mediastinum	Stage 2	(−)/(+)[1]
14	20 m/M	NA	NBL, Poorly diff., Low MKI, UH	Adrenal	Stage 3	(+)

m, months; y, years; M, male; NA, not amplified; A, amplified; NBL, neuroblastoma; nGNB, nodular ganglioneuroblastoma; MKI, mitosis-karyorrhexis index; FH, favorable histology; UH, unfavorable histology; (+), positive; (−), negative.
[1]Neuroblastoma component showed negative of TSLC1 signals, whereas ganglioneuroma showed positive of TSLC1 signals.

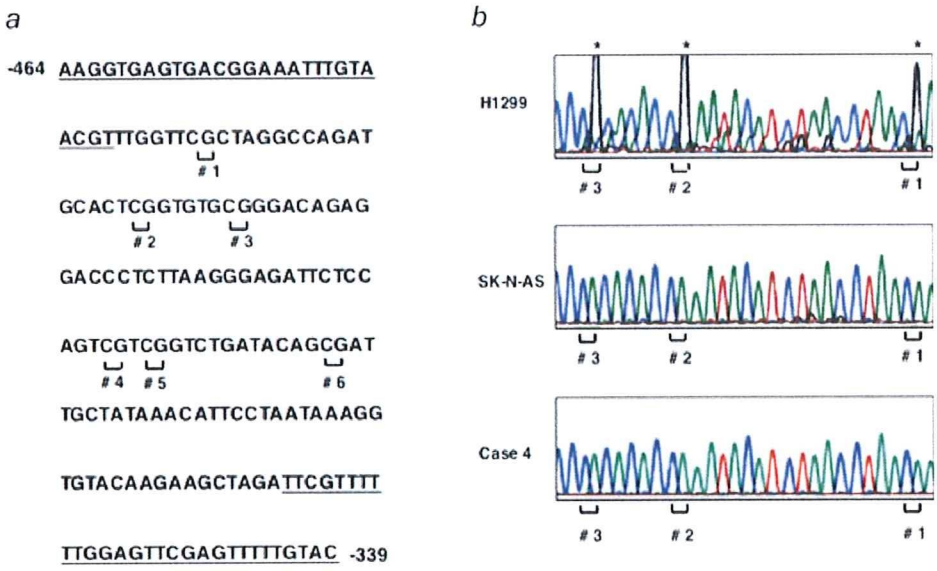

FIGURE 3 – Bisulfite-sequencing analysis of *TSLC1* gene promoter in neuroblastoma-derived cell lines and primary neuroblastomas. (*a*) Nucleotide sequence spanning from −464 to −339 relative to the translational initiation site (+1). Six CpG sites are shown. Primer sequences used for PCR-based amplification are underlined. (*b*) Bisulfite-sequencing analysis. Sequencing histograms showing the methylation status of CpG sites (#1, #2 and #3) are depicted. Asterisks indicate the positions of the methylated cytosine residues at the indicated CpG sites. H1299 cells were used as a positive control. [Color figure can be viewed in the online issue, which is available at www.interscience.wiley.com.]

in Kaplan-Meier cumulative survival curves (Fig. 2*b* and Supplementary Table I). Additionally, multivariable Cox analysis demonstrated that only clinical stage and *MYCN* amplification are significantly associated with their survival (Supplementary Table II), suggesting that *TSLC1* expression levels strongly correlate with these factors.

To further confirm the expression levels of TSLC1 in primary neuroblastomas, we employed immunohistochemical staining of TSLC1 in 11 primary neuroblastomas, including 5 favorable neuroblastomas bearing single copy of *MYCN*, 3 unfavorable neuroblastomas carrying single copy of *MYCN* and 3 unfavorable neuroblastomas with *MYCN* amplification. As shown in Figure 2*c*, TSLC1 appeared to be detectable at the cell–cell boundary of the tumors (cases 5 and 14) but not in Case 11. The immunohistochemical data were summarized in Table II. TSLC1 was detectable in tumors with favorable histology bearing single copy of *MYCN* (cases 4–8), whereas cases 9–11 with unfavorable histology carrying *MYCN* amplification did not express TSLC1. In addition, Case 13 was a nodular ganglioneuroblastoma whose ganglioneuroma and neuroblastoma components were TSLC1-positive and -negative, respectively. Of note, TSLC1 was detected in tumors with unfavorable histology bearing single copy of *MYCN* (cases 12–14). These observations indicate that there exists an inverse relationship between the expression levels of TSLC1 and *MYCN* amplification in primary neuroblastomas.

No promoter methylation of TSLC1 gene in neuroblastoma cell lines and primary neuroblastomas

Based on our present results, lower expression levels of *TSLC1* gene in unfavorable neuroblastomas might not be due to allelic loss of *TSLC1* locus. Since accumulating evidence strongly suggests that the downregulation of *TSLC1* in several cancers is associated with the hypermethylation of its promoter region,[9,11,12,24,26–29] we sought to examine whether the hypermethylation of *TSLC1* promoter region could be detectable in unfavorable neuroblastomas. For this purpose, we directly examined the methylation status of 6 cytosine residues of CpG sites within a putative *TSLC1* promoter region (Fig. 3*a*) by bisulfite-sequencing in 27 cell lines and 115 primary neuroblastomas. Sodium bisulfite modification of genomic DNA converts unmethylated cytosine residues to uracil residues but does not affect methylated cytosine residues. Unexpectedly, methylated cytosines